NATIONAL ADVISORY COMMITTEE FOR AERONAUTICS

PRELIMINARY INVESTIGATION DIRECTED TOWARD IMPROVEMENT OF THE NACA COWLING

By E. Floyd Valentine
Langley Memorial Aeronautical Laboratory

April 1942

NATIONAL ADVISORY COMMITTEE FOR AERONAUTICS

PRELIMINARY INVESTIGATION DIRECTED TOWARD IMPROVEMENT OF THE NACA COWLING

By E. Floyd Valentine

SUMMARY

The development of new cowlings, applicable to a short-nose radial engine, is described. These cowlings, designated the NACA cowlings D_s and D_{sf}, employ a larger spinner and a higher inlet-velocity ratio than does the conventional NACA cowling C.

The pressures available for cooling and the estimated critical Mach number were found to be higher with the new cowlings than are usually encountered with the conventional NACA cowling C.

Large-chord propeller cuffs were found to have a stabilizing effect on the flow entering the cowling and resulted in increased front pressures. Fan blades mounted on the spinner in the inlet opening had a similar effect.

INTRODUCTION

The present trend in airplane development is toward the attainment of the utmost speed at increasingly high altitudes. This increased performance is in part made possible by the development of more powerful engines supercharged to deliver rated power at high altitudes. Because of the increase in speed and altitude and the change in engine-cooling requirements, the demands on the cowling become more difficult to meet and certain cowling characteristics that did not require consideration in earlier cowling development become important.

The present tests are a continuation of a previous program that resulted in the development of a cowling especially for radial engines equipped with long-nose propeller-drive shafts. These tests were made at the

Langley Memorial Aeronautical Laboratory, Langley Field, Va. The basic work conducted on the model airplane in the propeller-research tunnel of the NACA has not been published; the work done in the full-scale tunnel of the NACA is reported in reference 1.

The investigation reported herein was directed toward the improvement of the conventional NACA cowling with respect to (1) drag due to external flow, (2) drag due to losses associated with cooling, (3) cooling, (4) critical speed, and (5) net efficiency.

The excess drag is believed to arise from various causes as follows:

(a) Spillage of air out of the inlet opening results in a poor recovery of energy in the wake, particularly for bodies of low fineness ratios.

(b) Turbulence within the cowling causes a loss in energy that shows up as a drag increase and as a loss in pressure available for cooling.

(c) High local velocities (high peak negative pressures) over the cowling surface result in high local skin friction and losses from incomplete transformation of the velocity energy back into pressure energy. Critical-speed limitations are also indicated.

(d) The propeller hub and the blade shank have been found to be a source of power loss even though they operate in the reduced-velocity region at the inlet of the conventional cowling. The cooling in many cases has not been satisfactory owing to the low front pressures arising from turbulence and spillage and because of the absence of propeller-shank fairings. Average front pressures generally range between 0.8q and 0.9q and are not uniform over the engine.

The methods used in this investigation to improve the flow conditions are outlined as follows:

(a) With large spinners having relatively small cowling-inlet areas, the inlet velocity was varied to determine the conditions necessary to stabilize the flow entering the cowling. The external shapes were

successively modified in order to increase the critical speed by reducing the external pressure peaks.

(b) Large spinners and blade-shank fairings were utilized to reduce the power losses of the propeller and to increase the front pressures.

(c) With a larger inlet area, the effect on the flow conditions of fan blades in the cowling inlet was investigated.

The tests consisted primarily of pressure measurements and flow studies made with a 0.4-scale model. The actual effect on airplane and engine performance resulting from the improved flow is yet to be determined.

COWLING DESIGNATIONS

The recent development of several new cowling types has necessitated the use of a suitable system of identification. In reference 2, the term "cowling C" was applied to the best nose-profile shape developed for the conventional NACA cowling. Owing to the wide use of this profile, the conventional NACA cowling is now generally referred to as "NACA cowling C." For convenience it has been decided to continue the use of letters as a means of identifying the newer types. With C for the conventional cowling, the new types will be denoted by succeeding letters of the alphabet in the order of their development. Minor variations of a particular type will be indicated by suitable subscripts.

Figure 1 shows the three types of cowling that have been developed to date. Cowling D is characterized in general by an annular inlet opening through which air is admitted at a relatively high inlet velocity with respect to the flight speed. The present paper deals with the development of two forms of this type, D_s and D_{sf}, in which the subscript s refers to a design applicable to short-nose engines and f indicates the use of a fan at the cowling entrance. The subscript l in D_l, shown in figure 1, indicates a design suitable for long-nose engines.

Cowling E employs a hollow spinner through which

both cooling and accessory air may be admitted. The external profile of this cowling is designed to eliminate completely the occurrence of a negative pressure peak, thereby permitting a high critical compressibility speed. A previous development referred to as a "nose blower" (reference 3) was similar in that air was admitted through a hollow spinner. The external lines for cowling E may be obtained from reference 4. In designs in which the spinner is large enough relative to the propeller, cuffs may not be required with cowling E.

SYMBOLS

H/q	total-pressure coefficient
p/q	static-pressure coefficient
$\Delta p/\rho n^2 D^2$	pressure-drop coefficient with propeller operating
v/V	velocity ratio
A/F	duct area in terms of engine frontal area
K	conductivity of engine or orifice plate $\left(\frac{Q}{FV\sqrt{\Delta p/q}}\right)$
V/nD	advance-diameter ratio of propeller
C_P	power coefficient $(P/\rho n^3 D^5)$
C_{T_n}	net thrust coefficient $\left(\frac{R+D_{st}}{\rho n^2 D^4}\right)$
η_n	net efficiency $\left(\frac{C_{T_n}}{C_P}\frac{V}{nD}\right)$
Δp	pressure drop through a resistance
q	dynamic pressure in free stream
H	total pressure measured above free-stream static pressure

V	free-stream velocity
v	velocity in a duct
ρ	mass density of air
A	duct area
F	engine frontal area
Q	volume rate of internal flow per unit time
n	propeller revolutions per unit time
D	propeller diameter
P	power applied to propeller
R	resultant force in thrust direction measured during test
D_{st}	drag of model with streamline nose

Subscripts i and e refer, respectively, to average conditions at the air inlet and at the air exit. Subscript t refers to average conditions in the duct at the location of the front tubes. (See fig. 5.)

APPARATUS AND METHODS

The experiments were performed in the propeller-research tunnel of the NACA.

The modified 0.4-scale model of the pursuit airplane, on which the tests were made, is shown in figure 2. In the course of the preliminary runs, the sides of the model were altered as shown in figure 3. With the sides altered, two adjustable doors were used for the cooling-air exit in order not to interfere with the oil-cooler and carburetor-air systems. The inlet-velocity ratio was varied by changing the opening of these doors.

A calibrated electric motor inside the model turned the right-hand, three-blade, 4-foot-diameter metal propeller shown in figure 2. The geometric characteristics of

the propeller blade and of the cuffs are shown in figure 4. The cuffs were of sheet metal with a symmetrical section at the spinner tapering to a section fitting the propeller at the 0.5 radius.

The engine was simulated by an orifice plate having a large number of $\frac{1}{2}$-inch-diameter holes distributed over an area similar to the area within which the cooling air actually enters the cylinder-baffle system of the full-scale airplane. The conductivity of the orifice plate was 0.10. Details of the orifice plate are given in figure 5, which also shows the pressure-tube arrangement for measuring the cooling-air flow. The front tubes of figure 5 were used to give an indication of the cooling-air flow distribution around the entrance. The tubes for measuring the pressure on the front of the plate were located as shown in figure 5 relative to the holes in order to avoid erroneous readings due to flow angularity. The rear pressure was obtained from a tube in an undisturbed region back of the plate.

In addition to the provisions for engine-cylinder cooling, inlet openings were provided for air to an oil cooler, a carburetor, and two intercoolers. From each of these inlet openings the air was conducted through a screen and then out through an adjustable slot. The primary object of these auxiliary-air systems was to provide inlets in suitable locations in order to simulate the actual conditions of operation for the cowling. Little attempt was made to simulate the internal ducts required for an actual installation. Each of the auxiliary-air systems had a total-pressure and a static-pressure tube immediately ahead of the screen to indicate the quantity of air flowing, a total-pressure tube in the entrance, and a total-pressure tube back of the screen.

The shape of cowling D_s arrived at in the tests is shown in figures 6 and 7. Figure 8 shows the arrangement for tests using fan blades to equalize the distribution of flow into the inlet slot. This cowling arrangement was identical with D_s arrangement except for the decrease in spinner radius near the inlet and the consequent increase in inlet area of about 50 percent. The openings for oil-cooler, carburetor, and intercooler air are shown in figures 6 and 7. The ordinates for the cowling lines of figures 6 to 8 are given in table I.

Flush pressure orifices were installed along one side of the cowling and along the top of the carburetor-air-duct outer cover to give the pressure distribution near the lip of the cowling.

The operating conditions assumed for the full-scale airplane were

V = 350 miles per hour or 513.5 feet per second

Altitude = 16,000 feet

For the engine,

K = 0.10

Δp = 8 inches of water or 41.7 pounds per square foot

$F = \pi/4\ (4)^2$ = 12.57 square feet

For the oil cooler,

K = 0.46 (based on full-scale 10-inch-diameter oil cooler)

Δp = 8 inches of water or 41.7 pounds per square foot

The volume rate of flow was assumed to be the same for the oil cooler as for the carburetor. It was estimated that each intercooler would use an amount of air equal to 80 percent of the amount of air supplied to the carburetor.

The corresponding values for the 0.4-scale model are then

For the engine,

$F = 0.16 \times 12.57 = 2.01$ square feet

$$\Delta p/q = \frac{(41.7)\ (2)}{(0.002378)\ (0.6088)\ (513)^2} = 0.219$$

$$Q = KAFV\sqrt{\Delta p/q} = 0.1 \times 2.01\sqrt{0.219}\ V = 0.0940V$$

$$A_i = \frac{Q}{v_i} = \frac{0.0940}{v_i/V}$$

For the oil cooler,

$Q = 0.46\ \pi/4\ (10/12)^2 = 0.0188V$

For each intercooler,

$Q = 0.80 \times 0.0188V = 0.0150V$

RESULTS AND DISCUSSION

Tests with no propeller.- A number of cowling-spinner combinations of the D_s type were tested over a wide range of inlet-velocity ratios. The most promising combinations were tested more thoroughly, the tests including external-pressure-distribution measurements to indicate the probable critical speeds. The results of the tests of only the most effective arrangements are presented in this report.

In order to obtain satisfactory ground cooling, the inlet opening was located at as great a radius as possible without increasing the negative peak pressures over the cowling lip.

Stabilized flow at the inlet was obtained with cowling D_s when the inlet-velocity ratio was 0.5 or greater. Reduction of the inlet velocity or modification of the spinner in such a way as to increase the thickness of its boundary layer caused a flow breakdown in the diffuser. The pressures on the front of the orifice plate also dropped from 1.0q to about 0.8q.

The spinner was given a reflex curvature in order to thin out the boundary layer and to obtain as favorable a pressure gradient at the entrance as possible. Figure 9 gives the pressure distribution measured on the spinner surface. The front portion of the spinner surface was made to approximate a spherical surface that would permit the front part of the cuffs to be closely fitted.

The extremes in velocity indicated by the front tubes of figure 5 are shown in figure 10. If the velocity distribution around the inlet were uniform at this section, the maximum and the minimum v/v_t would be equal and would have a value greater than unity because of the radial velocity variation in the inlet. These data show that, at inlet-velocity ratios below 0.5, the flow is not uniform for either spinner. Above an inlet-velocity ratio of 0.5, the flow is more nearly uniform for the short spinner than for the long spinner.

The preliminary tests indicated that the entrance area could not be reduced much below that shown in figure 6 without increasing the losses in the diffuser to a prohibitive extent. Two angles of divergence between the inner and the outer duct surfaces, 5° and 8°, were tried. The 5° angle appeared to be the most favorable for this particular cowling and was used for all the ensuing tests. The expansion was increased rapidly in the last quarter of the distance from the inlet to the orifice plate in order to cover the engine cylinders.

Figures 11 and 12 show the pressure distribution on the front of the plate for both spinners. With no propeller and no losses from the boundary layer on the spinner or from diffusion in the inlet, the curves would all be at a p/q of 1.0. From these figures it appears that, for inlet-velocity ratios below 0.54 for the long spinner and 0.52 for the short spinner, conditions are not uniform around the spinner. Either the pressure distribution on the plate or the uniformity of the velocity measurements in the inlet gives an indication of the quality of the flow. On the basis of the pressure distribution on the orifice plate, there is not, however, as much improvement indicated by the use of high inlet-velocity ratios as was indicated by the velocity measurements in the inlet. This difference is to be expected, of course, because the front pressures show the net effect of the uniformity of the entrance flow plus the losses in diffusion, which increase, approximately, as the square of the inlet velocity.

The pressure distribution on the plate is more nearly uniform and the pressure is higher for the short spinner than for the long spinner at any given inlet-velocity ratio. The peak pressures on the cowling, however, would have to be taken into account in choosing between the two. Figures 13 and 14 show the effect of the spinner shape on the pressure distribution over the cowling surfaces. The spinner size has a pronounced effect on the pressures over the cowling. The long spinner gave the lower pressures.

In order to lower the peak pressures shown in figure 13, the carburetor-air-duct lip was lowered to get the effect of a reduction in the angle of attack. The surface was then progressively reworked to the shape given in table I. The pressure distributions for the reworked shape are shown in figures 15 and 16.

The effect of a 10° angle of attack on the pressure

distribution over the top of the cowling is shown in figure 17. Figure 18 shows that the angle of attack had only a small effect on the pressures over the side of the cowling.

Tests of cowling D_s with propeller.- The long spinner was used for the propeller tests because the short spinner, being built of wood and plaster of Paris, could not be used with the propeller. Two flight conditions were simulated in the final tests. In order to represent the high-speed condition, a propeller setting of 37.1° at the 0.75 radius was used with an angle of attack of the thrust line of 0°. The oil-cooler and the carburetor-air exit flaps were set for approximate inlet-velocity ratios of 0.5 at the high-speed V/nD. For the take-off condition, a propeller setting of 20° and an angle of attack of 10° were used. The oil-cooler exit flap was opened to a 20° position. The cooling-air exit doors were set approximately 40° to the model surface.

Figure 19 shows that, with the propeller operating, the pressure distribution on the plate does not change much with the inlet-velocity ratio over the small range covered. On the basis of the indicated inlet-velocity variation as shown in figure 10 or the pressure distribution on the orifice plate, the effect of the propeller is to permit operation at a lower inlet-velocity ratio than appeared desirable from the results obtained without the propeller. The exit area was adjusted on the basis of the indicated inlet-velocity variation to a value which gave an inlet-velocity ratio of 0.54 at the high speed V/nD.

For the high-speed condition, figure 20 gives indicated values of pressure drop through the screen and velocity and total pressure in front of the screen for the auxiliary internal-air systems. Figure 21 shows the cooling-air pressure-drop coefficient and the corresponding inlet-velocity-ratio curve. Curves for the front pressure on the plate and the pressure drop are also given in terms of the free-stream dynamic pressure. The pressure-drop and the inlet-velocity curves are determined by the pressure-drop coefficient at any given value of V/nD.

The relations for determining the curves are

$$\frac{\Delta p}{q} = \frac{2\,\frac{\Delta p}{\rho\, n^2\, D^2}}{\left(\frac{V}{nD}\right)^2}$$

and

$$\frac{V_i}{V} = K\,\frac{\bar{F}}{A_i}\sqrt{\frac{\Delta p}{q}}$$

The pressure distribution on the front of the orifice plate is given in figure 22 for a V/nD of 1.5. Over most of the orifice-plate area the cuffs have increased the total pressure by more than the amount lost in the diffuser ahead of the plate.

The pressure-drop coefficient and the entrance-velocity ratio are given in figure 23 for the take-off condition. The derived curve of $\Delta p/q$ is drawn in at the higher values of V/nD. Figure 24 was prepared from the pressure-drop-coefficient curve of figure 23, since the quantity $\Delta p/q$ becomes meaningless at low speeds. Figure 24 applies only to the geometrically similar full-scale airplane with a 10-foot propeller. The pressure distribution over the front of the plate at a V/nD of 0.65 is given in figure 25. The propeller has a large effect on the pressures on the front of the orifice plate, as would be expected. The variation in pressures around the orifice plate is caused by the angle of attack of the model, which has the effect of increasing the local angle of attack of the cuff sections going down on the right side and decreasing the angle of attack of the cuff sections going up on the left side.

It may be interesting to note that increasing the angle of attack from 0° to 10° decreased the pressure behind the baffle plate by $0.3q$. This effect may be accounted for by the low pressure field of the wing extending to the doors.

Tests with axial fan to prevent reverse flow, cowling D_{sf}.- For the cowling D_{sf} arrangement it was intended that, at the high-speed condition, the fan blades mounted on the spinner should control the flow into the inlet rather than help force the air through the cooling system. It was assumed that, if the blade angle were adjusted to

approximately zero lift under the high-speed operating conditions, the power absorbed by the fan blades would be very small and that any local deviation from uniform flow into the inlet would change the angle of attack of each blade as it passed the disturbed section in the direction to oppose the deviation while it was still small. The result should be to stabilize the velocity around the inlet to a uniform value.

The axial fan would also be advantageous in increasing the cooling flow for the ground and the climbing conditions, inasmuch as the angle of attack of the blades would increase as the quantity of cooling air decreased.

The larger inlet area of cowling D_{sf} was obtained by using the same outer cowling as for the D_s cowling tests with smaller spinner and inner-diffuser surface diameters. No alteration of the outside surface to obtain the lowest peak pressures for the D_{sf} cowling was attempted. Satisfactory measurements of the velocity distribution at the inlet were not obtained because of the difficulty in setting the front tubes of figure 5 relative to the flow back of the fan blades. The pressure distribution on the plate was therefore used to indicate the quality of the flow in the cowling.

Figure 26 shows the pressure-drop coefficient in the high-speed condition for two fan-blade settings with different values of the exit area. Values of exit area are given in figures 26 to 32 to separate the effects of the fan blades from the effects of internal-flow changes resulting from exit-area changes. The lines of constant $\Delta p/q$ are included to give the pressure-coefficient curves added significance. The $\Delta p/q$ curves are not plotted from test data since, for fixed values of $\Delta p/q$, a curve of $\Delta p/\rho n^2 D^2$ is determined. The 35° setting appears to be on the low side as it decreases the flow over most of the range. The 45° setting increases the flow over most of the range. It appears that a fan-blade setting of 40° would have given the desired effect of no change in flow caused by the blades in the high-speed condition.

Figures 27 to 29 give the pressure distribution on the plate at $V/nD = 1.5$ for various conditions of fan-blade setting and inlet-velocity ratio. Figures 27 and 28 show improvement of the pressure distribution on the plate for both fan-blade settings with the 45° setting giving

the highest pressures, indicating that the fan did help in stabilizing the flow for low inlet velocities. The pressures can exceed q even with no fan blades since the cuffs were in place for all fan tests. Figure 29 shows an increase in front pressure as the exit area is reduced. This result follows from the fact that a reduction in the amount of flow increases the angle of attack on the fan blades and on the inner end of the cuffs.

The effect of the fan blades on the propeller characteristics is shown in figure 30. The C_T and the η curves are of little significance because the exit-door settings were changed and because the model was in a more carefully prepared condition for the drag test with the streamline nose than for the propeller tests with fan blades. It is also probable that the cuffs were not set at the optimum angle. The important conclusion to be drawn from figure 30 is that the fan blades may be used with a negligible power expenditure.

For the take-off condition, figure 31 shows a slight increase in pressure coefficient for the 35° fan-blade setting and a considerable increase for the 45° setting. A poorer plate pressure distribution with fan blades is indicated in figure 32 for the take-off condition, although the average pressure and the volume of air flowing are definitely higher for the condition of blades set 45° than for the condition of no blades. This uneven pressure distribution may be accounted for by the angle of pitch, which has the effect of increasing the angle of attack of the blade and cuff sections going down on the right side and decreasing the angle of attack of the blade and cuff sections going up on the left side.

Comparison of cowlings D_s and D_{sf}.- It has been shown from these tests that, with no propeller, stable flow at the inlet may be obtained by the use of a high inlet-velocity ratio. The tests of cowling D_s with the propeller operating were made with an inlet-velocity ratio high enough to insure stable flow without the effect of the propeller cuffs. The possibility of using a lower inlet-velocity ratio with propeller operating was not investigated on cowling D_s. The inlet-velocity ratio for cowling D_{sf}, however, was considerably lower than for D_s, and the results obtained without the fan blades may be compared with the high inlet-velocity results of cowling D_s with propeller. This comparison is not strictly

valid since the optimum cuff setting for a cowling with low inlet-velocity ratio would not be the optimum setting for a cowling with high inlet-velocity ratio.

The pressures on the front of the plate are given in figures 33 and 34 for both the high-speed and the take-off conditions. The flow of air was substantially the same for the two cowlings. For the high-speed condition figure 33 shows that cowling D_{sf} without fan blades gives pressures on the front of the plate that approach in uniformity and magnitude the pressures obtained with cowling D_s, even though the inlet-velocity ratio is in the neighborhood of 0.3. In the take-off condition figure 34 shows the pressures with cowling D_{sf} without fan blades to be higher and more nearly uniform than with cowling D_s. The pressures exceed q for both cowlings because of the effect of the cuffs. The reason for the lower pressures with cowling D_s is that, with the higher inlet-velocity ratio, the losses in diffusion ahead of the plate are greater.

Figures 33 and 34 show that the effect of the fan blades on cowling D_{sf} was to increase the pressures on the front of the orifice plate for both the high-speed and the take-off conditions. In the take-off condition, however, the effect of the fan blades is also to make the pressure distribution on the plate less uniform.

Although no measurements were made of the surface pressures with cowling D_{sf}, it seems probable that the critical speed for cowling D_{sf}, either with or without the fan blades, could not be reduced to values obtainable with cowwling D_s.

CONCLUDING REMARKS

Flow and pressure studies leading to the development of NACA cowlings D_s and D_{sf}, designs that are applicable to short-nose radial engines, have been described.

Cowling D_s provided higher pressures for cooling at the front of the engine and had a higher estimated critical compressibility speed than is commonly expected with the conventional C-type cowling. These improvements were brought about through the use of a large spinner, a modi-

fied cowling shape, diffusion passages ahead of the engine, a relatively high inlet-velocity ratio, and the use of large-chord propeller cuffs.

Without the propeller, an inlet-velocity ratio of 0.5 was required to give stable flow into the cowling. With the stabilizing effect of the propeller equipped with large-chord cuffs, satisfactory pressure distribution on the front of the orifice plate was obtained with a larger inlet opening and an inlet-velocity ratio as low as 0.3. With the larger inlet opening, the pressures on the plate for the take-off condition were higher than with the smaller inlet opening owing to the decreased diffuser losses resulting from the lower inlet velocity.

Estimation of the critical speed from the peak negative pressures measured without the propeller gave a critical Mach number of 0.70 with the large spinner and an inlet-velocity ratio of 0.5 as compared with 0.63 for the C-type cowling.

Auxiliary ducts with inlets built into the cowling lip were found to provide full dynamic pressures without incurring surface pressures greater than those for the basic cowling.

Cowling D_{sf} had a larger inlet area than cowling D_s and had fan blades mounted on the spinner in the annular inlet. The fan blades had the same general effects as the cuffs; they provided stable inlet flow at an inlet-velocity ratio as low as 0.25 and increased the cooling pressures available in all flight conditions. The fan blades could be adjusted to absorb very little power in the high-speed condition.

This investigation should serve as a background for the development work necessary to each particular engine installation. The external shape required to give the lowest possible peak negative pressures varies with both the inlet size and the inlet-velocity ratio. The determination of this shape should, if possible, be made with propeller running for the design operating condition of each particular case. The effect of the spinner shape and size on the internal front pressures appears to be worthy of further experimentation and should be studied in the presence of the propeller.

Langley Memorial Aeronautical Laboratory,
National Advisory Committee for Aeronautics,
Langley Field, Va.

REFERENCES

1. Silverstein, Abe, and Guryansky, Eugene R.: Development of Cowling for Long-Nose Air-Cooled Engine in the NACA Full-Scale Wind Tunnel. NACA A.R.R., Oct. 1941.

2. Robinson, Russell G., and Becker, John V.: High-Speed Tests of Radial-Engine Cowlings. NACA A.C.R., April 1939.

3. Biermann, David, and Turner, L. I., Jr.: Ground-Cooling and Flight Tests of an Airplane Equipped with a Nose-Blower Engine Cowling. NACA A.C.R., Oct. 1939.

4. Becker, John V.: Wind-Tunnel Tests of Air Inlet and Outlet Openings on a Streamline Body. NACA A.C.R., Nov. 1940.

TABLE I

SPINNER AND COWLING ORDINATES OF COWLINGS D_s AND D_{sf}

[All ordinates given in inches]

Distance[a]	Spinner and inner cowling radii			Cowling			
	Long spinner, cowling D_s	Short spinner, cowling D_s	Long spinner with fan blades, cowling D_{sf}	Carburetor air duct ordinates in plane of symmetry		Circular-section radii	
				Inside	Outside	Inside	Outside
-10.87	0	----	0	----	----	----	----
-10.5	.50	----	.50	----	----	----	----
-10.0	1.14	----	1.14	----	----	----	----
-9.0	2.29	----	2.29	----	----	----	----
-8.5	2.75	0	2.75	----	----	----	----
-8.0	3.15	.97	3.15	----	----	----	----
-7.0	3.79	2.22	3.79	----	----	----	----
-6.0	4.33	3.14	4.33	----	----	----	----
-5.0	4.77	3.83	4.77	----	----	----	----
-4.0	5.12	4.31	5.12	----	----	----	----
-3.0	5.43	4.71	5.43	----	----	----	----
-2.0	5.68	5.23	5.68	----	----	----	----
-1.0	5.90	5.82	5.86	----	----	----	----
-.4	----	----	----	8.43	8.43	----	----
-.3	----	----	----	8.40	8.65	----	----
-.2	----	----	----	8.48	8.78	----	----
-.1	----	----	----	8.57	8.90	----	----
0	6.36	6.36	5.99	8.65	8.98	7.30	7.30
.1	----	----	----	----	----	7.19	7.54
.2	----	----	----	----	----	7.19	7.65
.3	----	----	----	----	----	7.24	7.76
.5	----	----	----	9.02	9.36	7.29	7.94
1.0	6.65	6.65	6.06	9.34	9.64	7.44	8.30
2.0	6.75	6.75	6.05	9.80	10.08	7.61	8.83
3.0	6.73	6.73	5.97	10.15	10.44	7.66	9.20
4.0	6.60	6.60	5.82	10.42	10.71	7.62	9.47
5.0	6.39	6.39	5.62	10.62	10.91	7.57	9.66
6.0	5.62	5.62	5.35	10.77	11.04	7.97	9.79
6.3	5.26	5.26	5.26	----	----	8.25	----
7.0	----	----	----	----	11.15	----	----
8.0	----	----	----	----	11.23	----	----
9.0	----	----	----	----	11.30	----	----
10.0	----	----	----	----	11.35	----	----

[a]Distances are measured along the thrust center line from station 0. Those distances given as negative are measured forward from station 0.

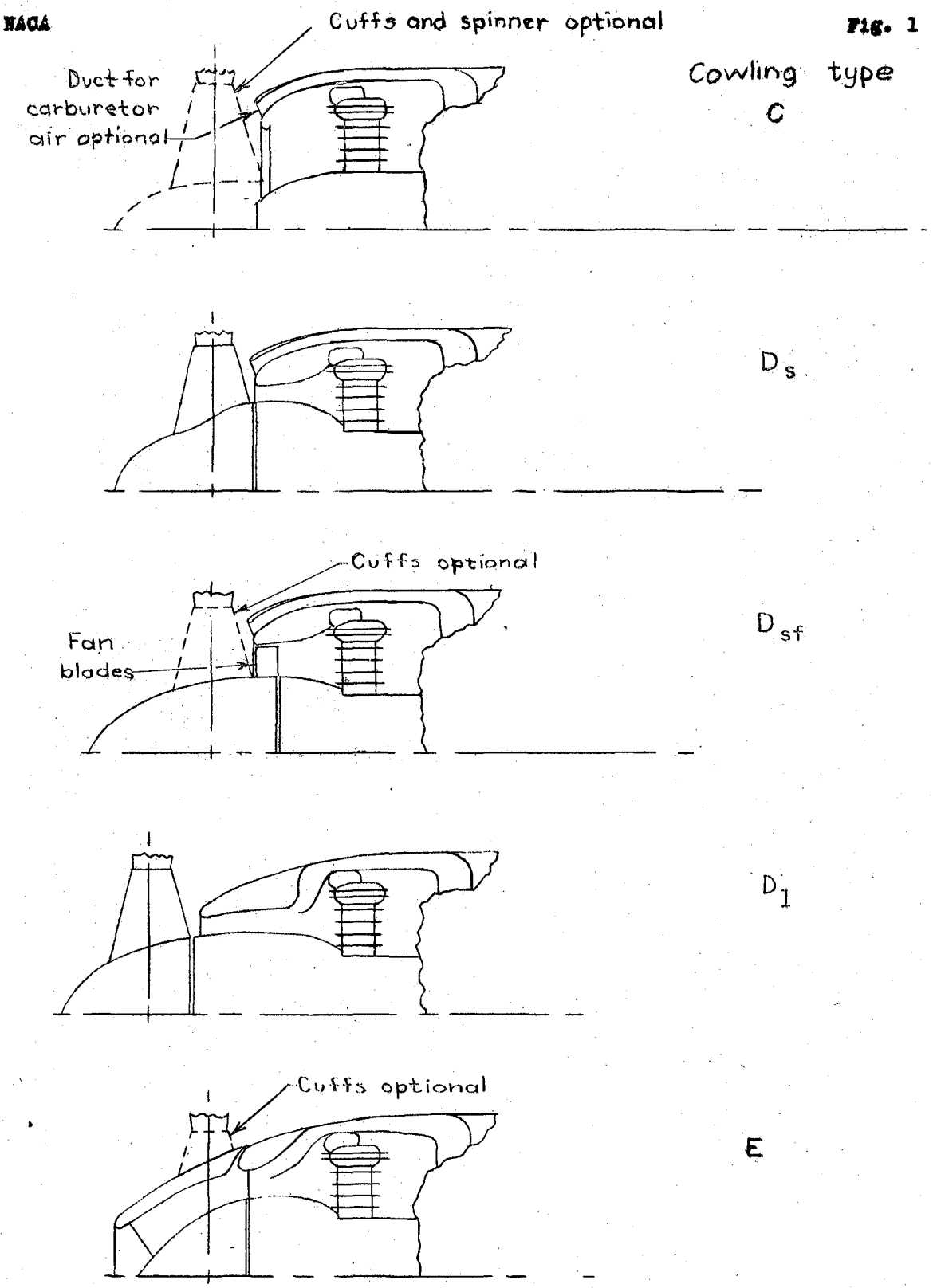

FIGURE 1.- NACA cowling-type designations.

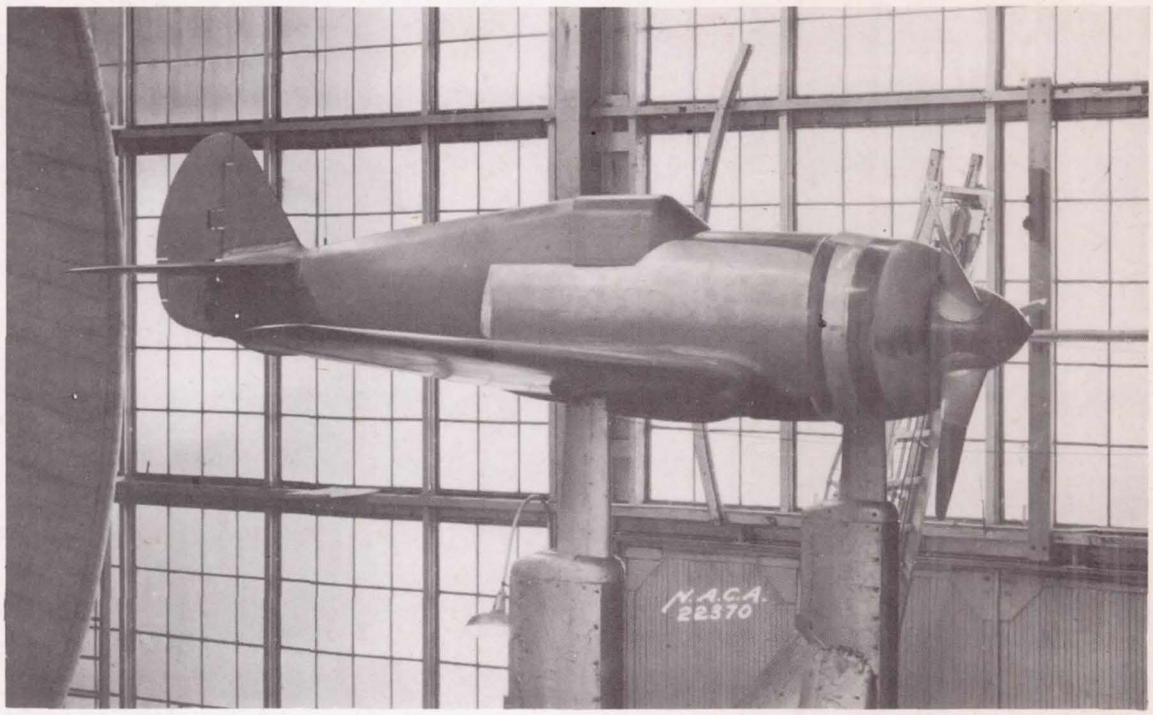

Figure 2.- Model in original condition before alteration to fuselage sides

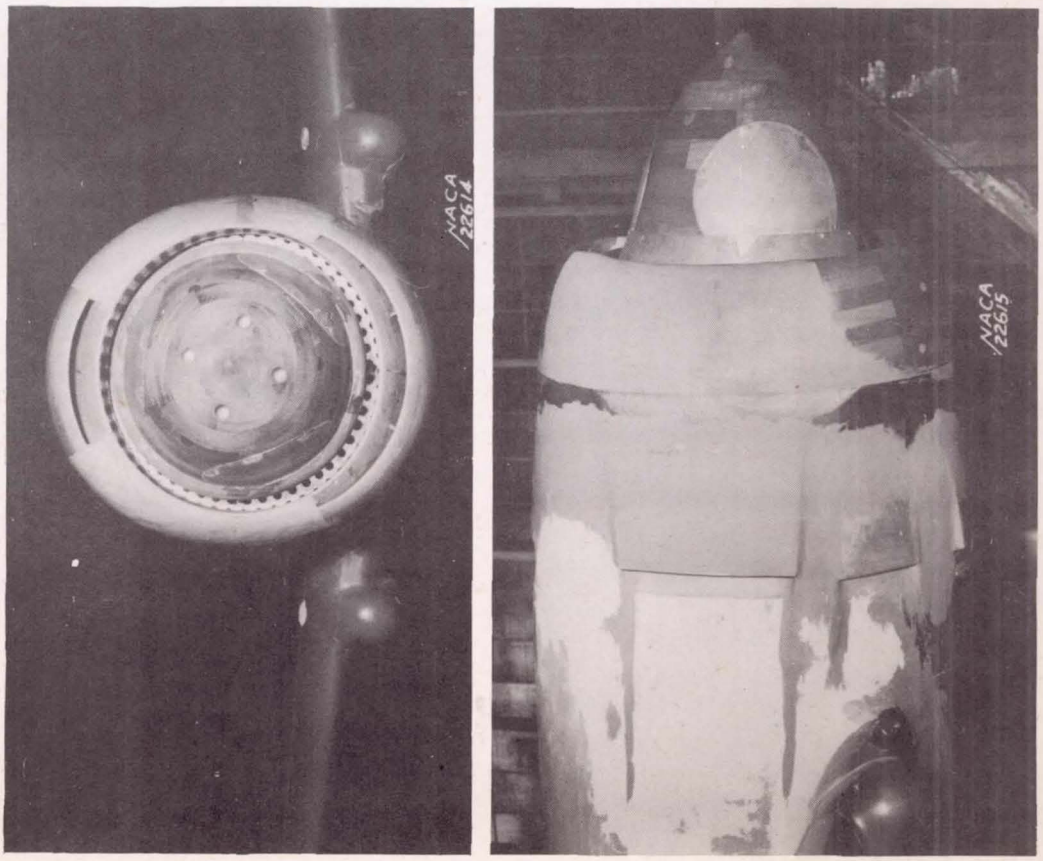

Figure 7.-Cowling D_8 with intake openings for carburetor air and cooling air to the oil cooler and to the intercoolers.

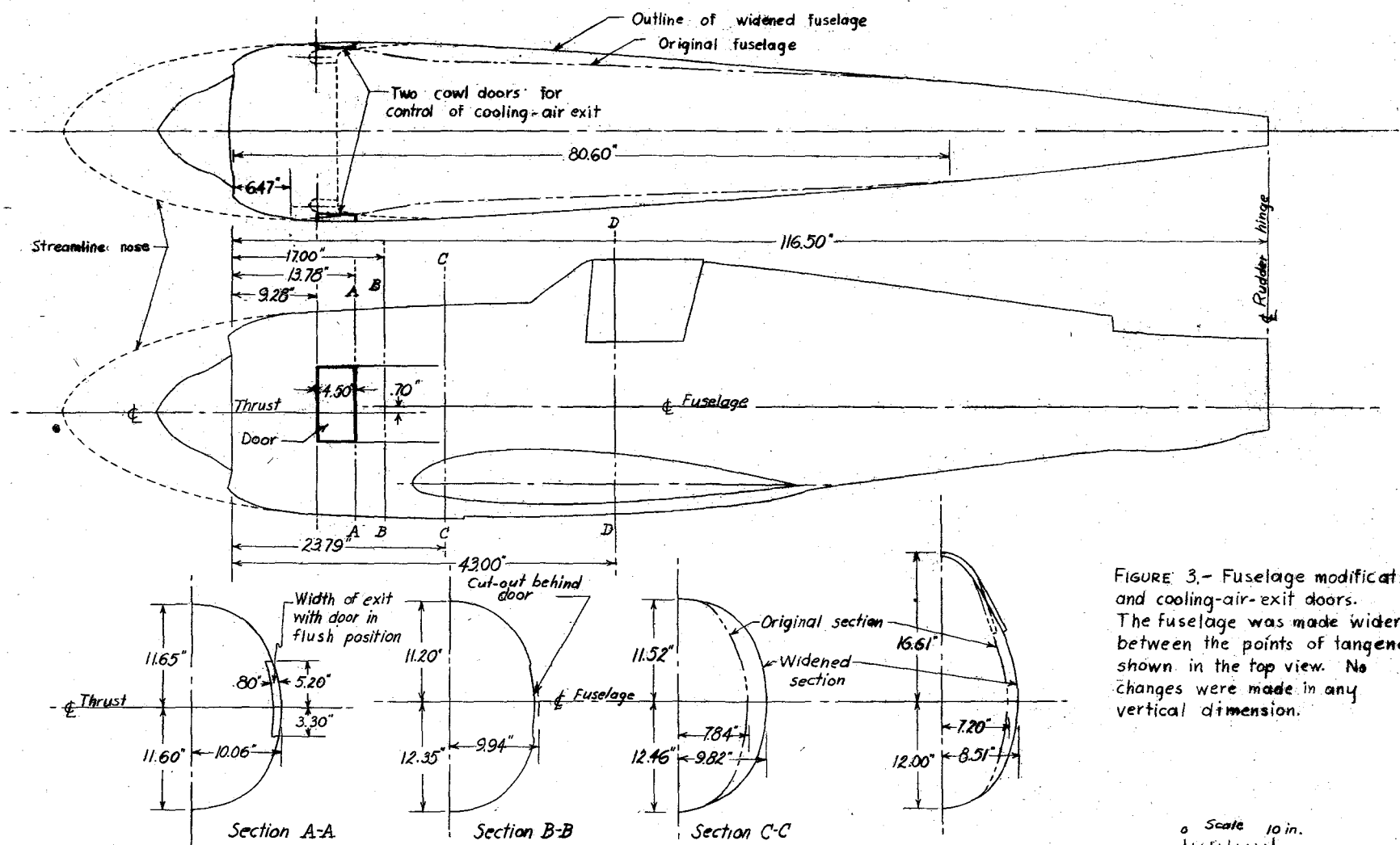

Typical Sections

FIGURE 3.- Fuselage modification and cooling-air-exit doors. The fuselage was made wider between the points of tangency shown in the top view. No changes were made in any vertical dimension.

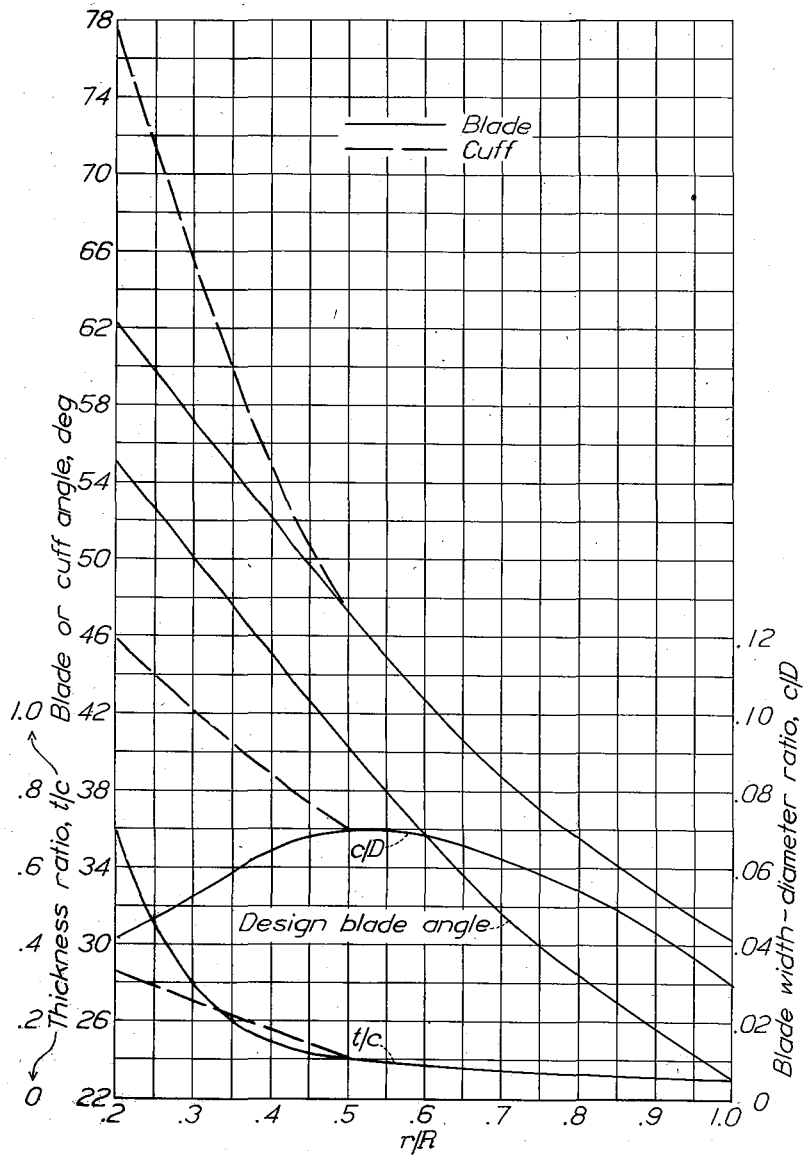

Figure 4.- Propeller blade shape and cuff shape. D, diameter; R, radius to the tip; r, station radius; t, section thickness; c, section chord. Hamilton Standard No. 6101A propeller.

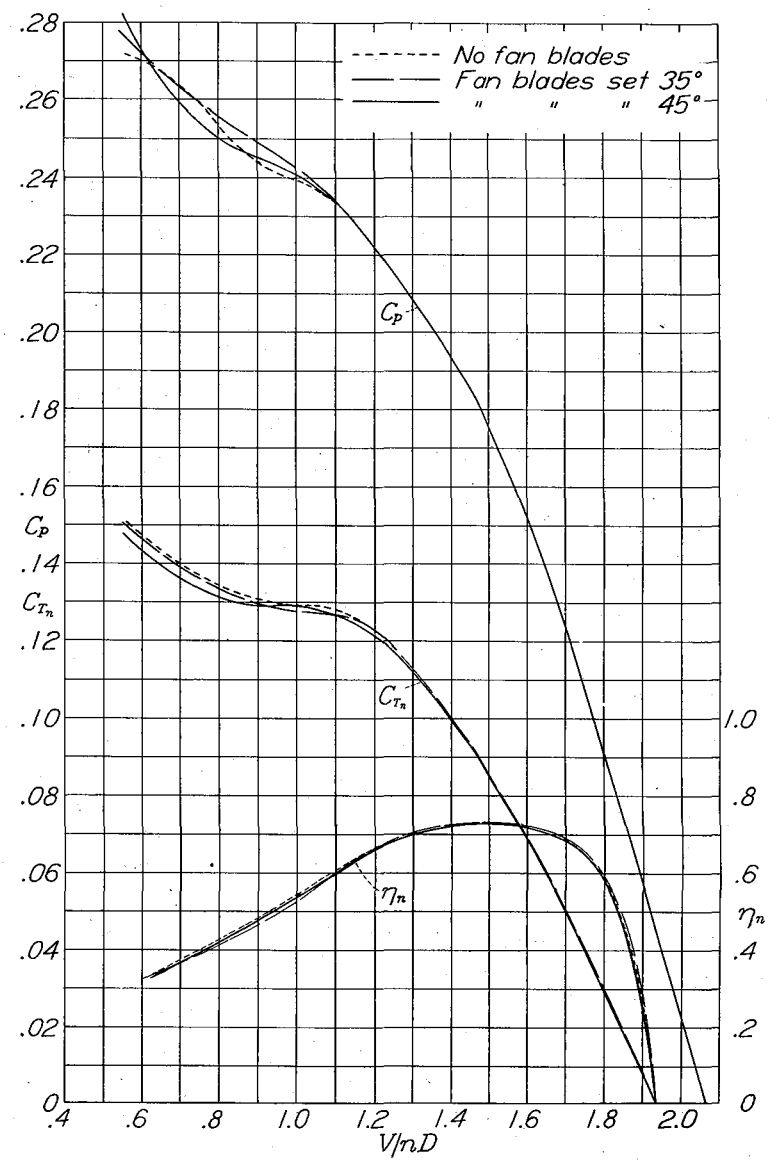

Figure 30.- Propeller characteristics for cowling D_{sf} including power used by fan blades. Propeller set 37.1° with cuffs; angle of attack, 0°; $A_e/F = 0.044$.

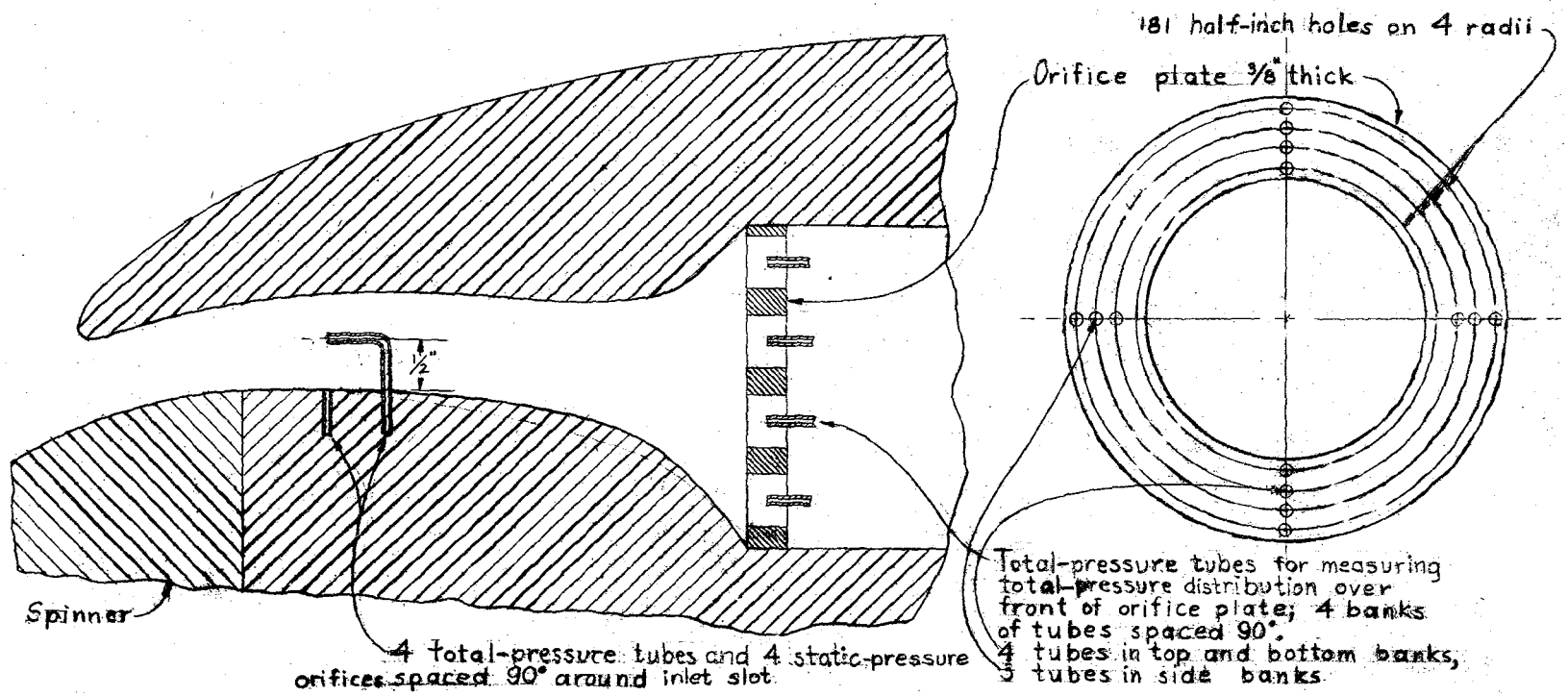

FIGURE 5 - Tube arrangement for measuring flow distribution in inlet and pressure distribution on front of static-pressure orifice plate.

Fig. 5

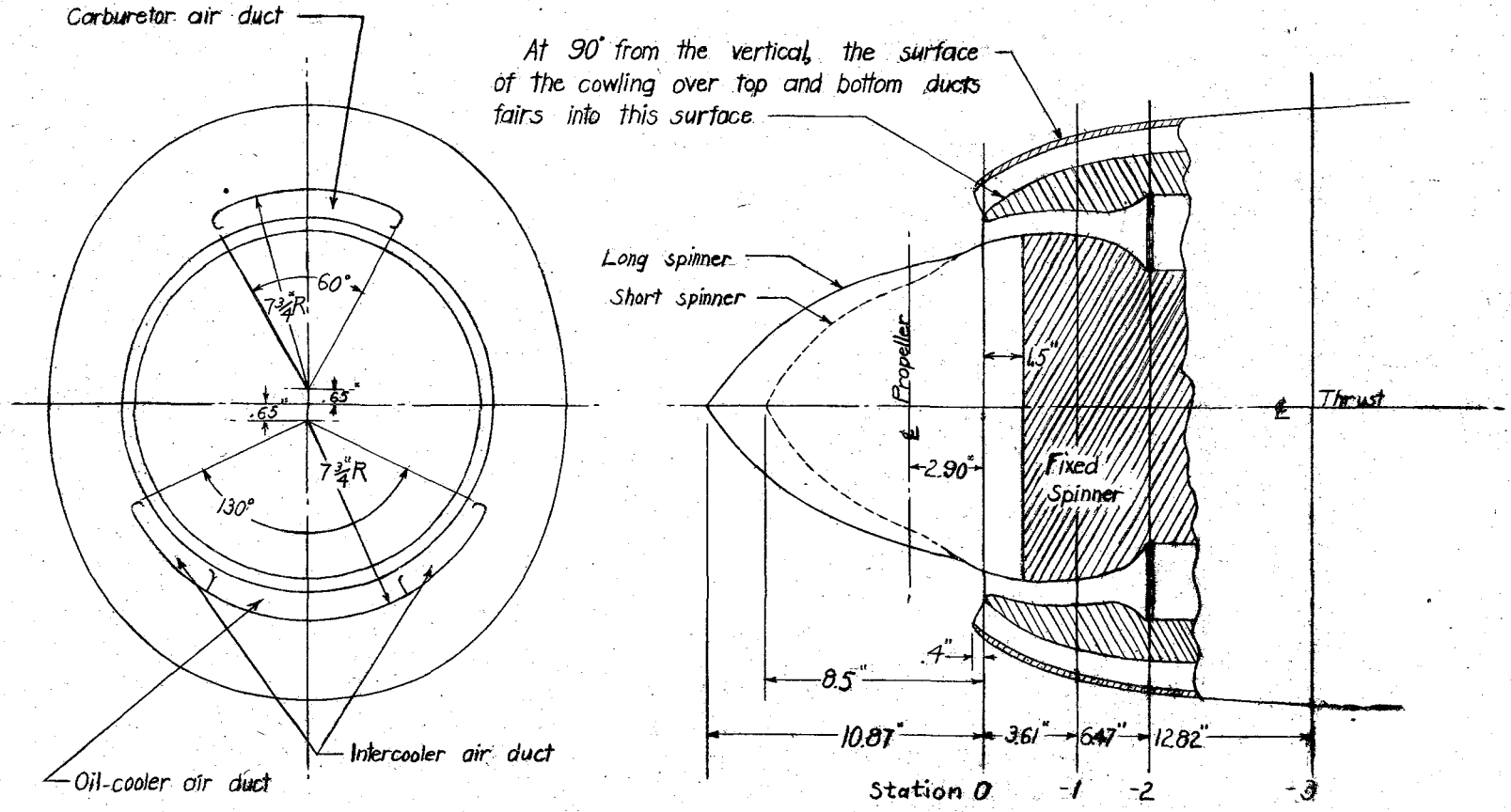

Figure 6.- NACA cowling D_s.

Ordinates for cowling and spinner given in table I

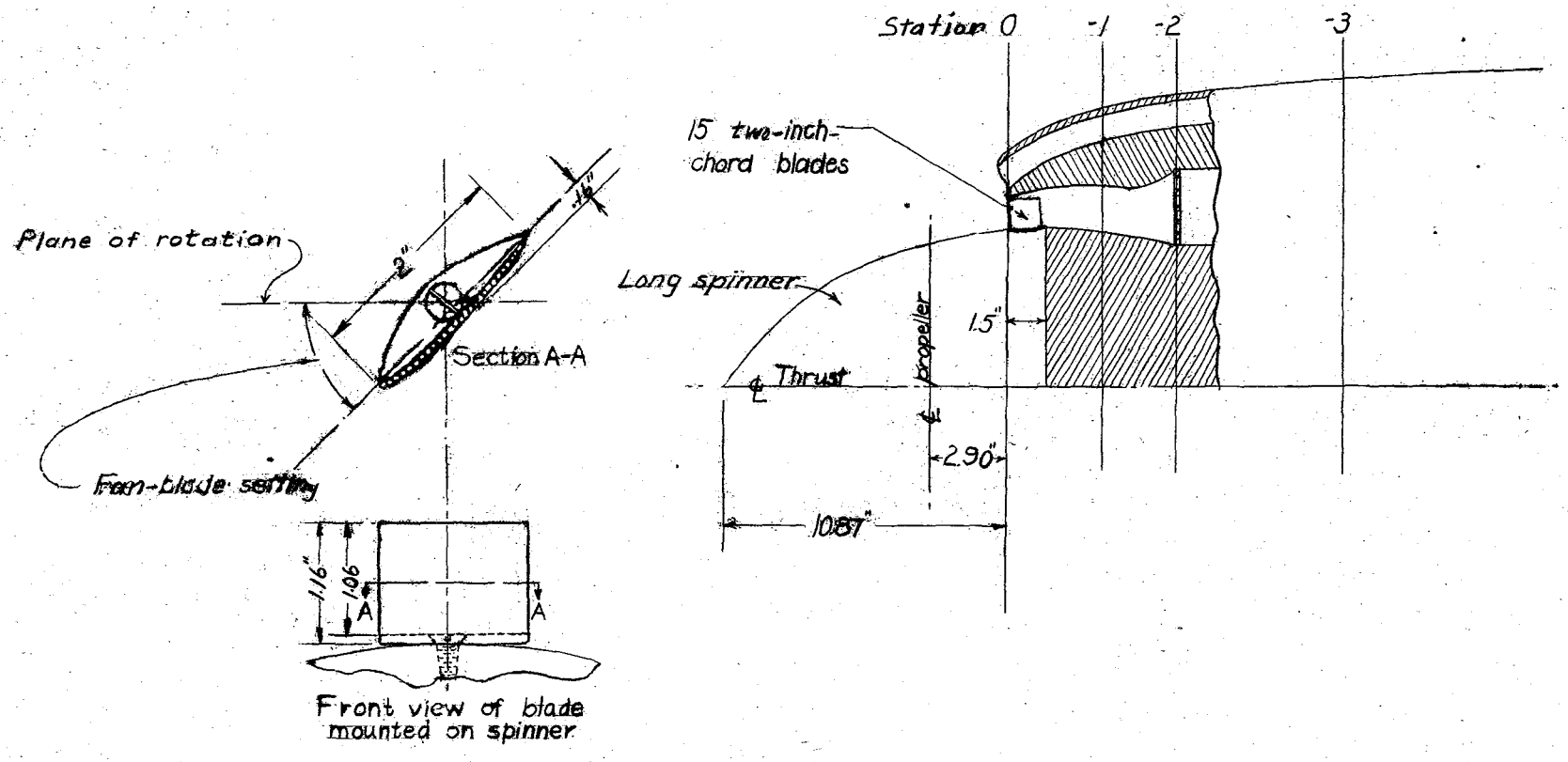

FIGURE 8 - Cowling arrangement used for tests with fan blades, cowling D_{sf}. Ordinates for spinner and inner cowling are given in table I.

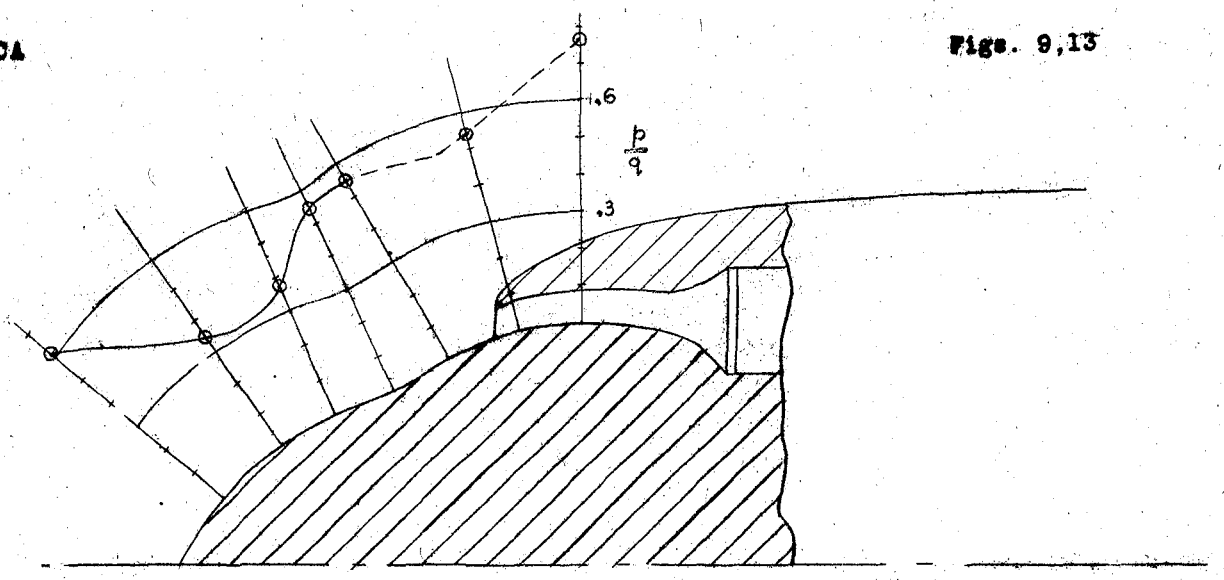

FIGURE 9.- Pressure distribution on side of short spinner. Angle of attack, 0°; v_i/V, 0.58.

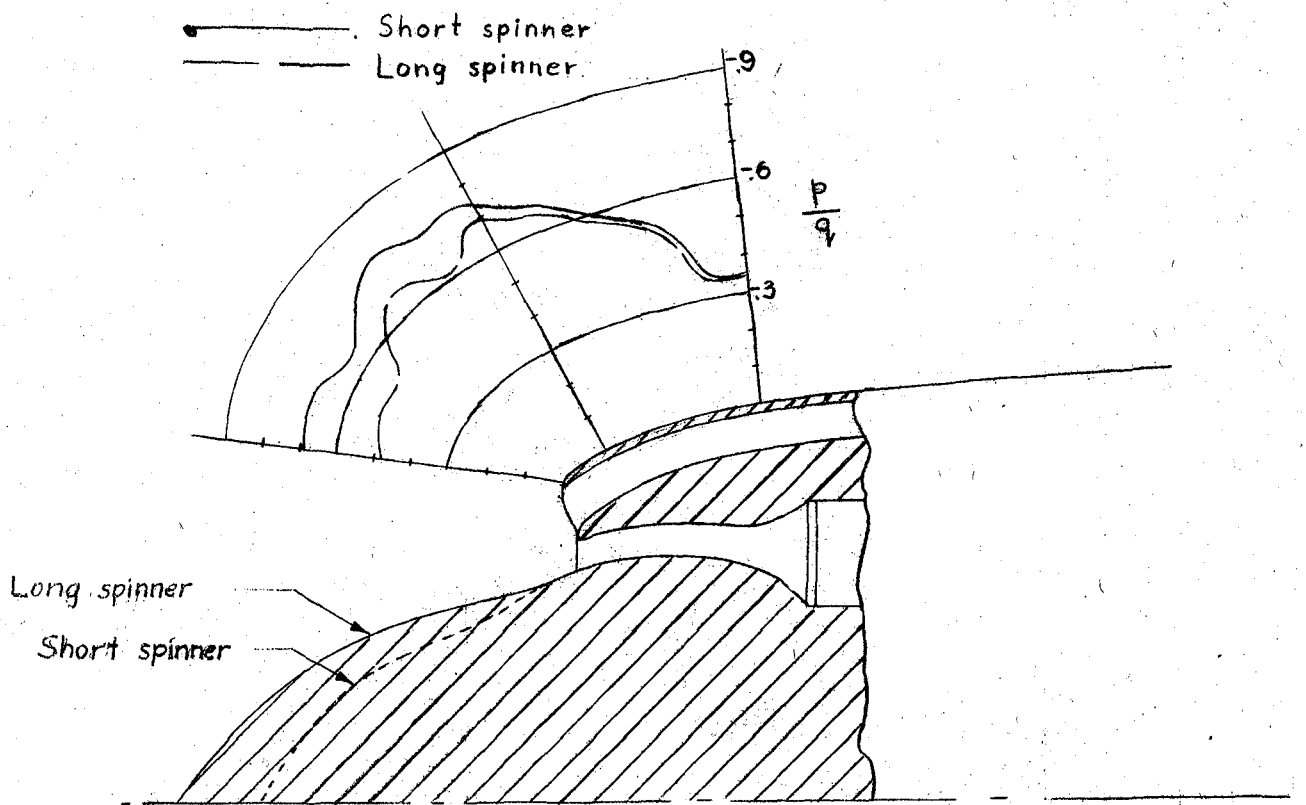

FIGURE 13.- Effect of spinner shape on pressure distribution over top of carburetor air duct. Angle of attack, 0°; v_i/V, 0.57. Pressures measured before maximum negative pressures were reduced by improving the outer lip shape.

(a) Short spinner, no propeller.

(b) Long spinner, no propeller.

(c) Long spinner, propeller set 37.1°; V/nD, 1.7.

Figure 10.- Effect of inlet-velocity ratio on range of velocities indicated by front tubes. Cowling D_s; angle of attack, 0°.

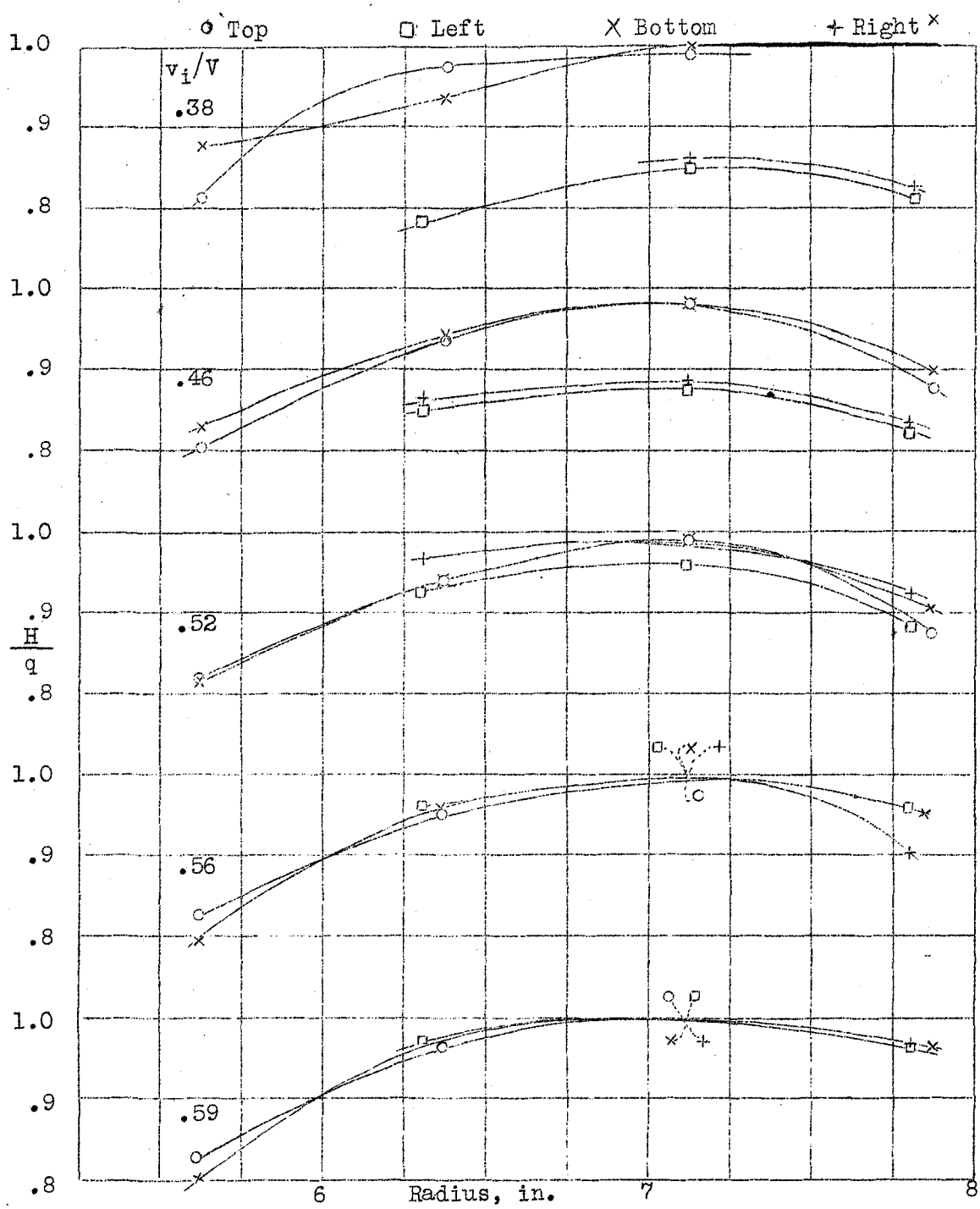

Figure 11.- Pressure distribution on orifice plate. Cowling D_s; no propeller; short spinner; angle of attack, 0°.

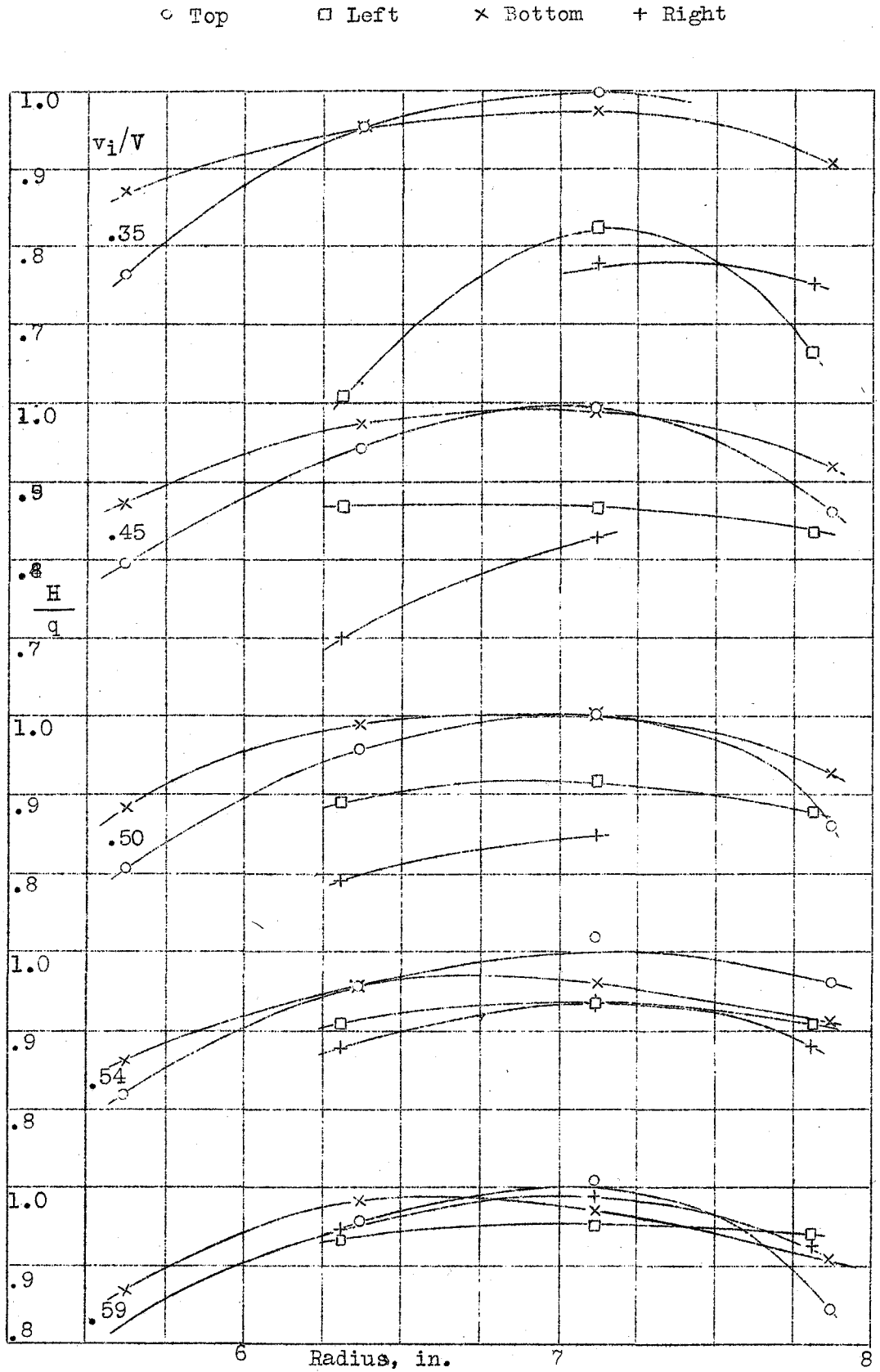

Figure 12.- Pressure distribution on orifice plate. Cowling Ds; no propeller; long spinner; angle of attack, 0°.

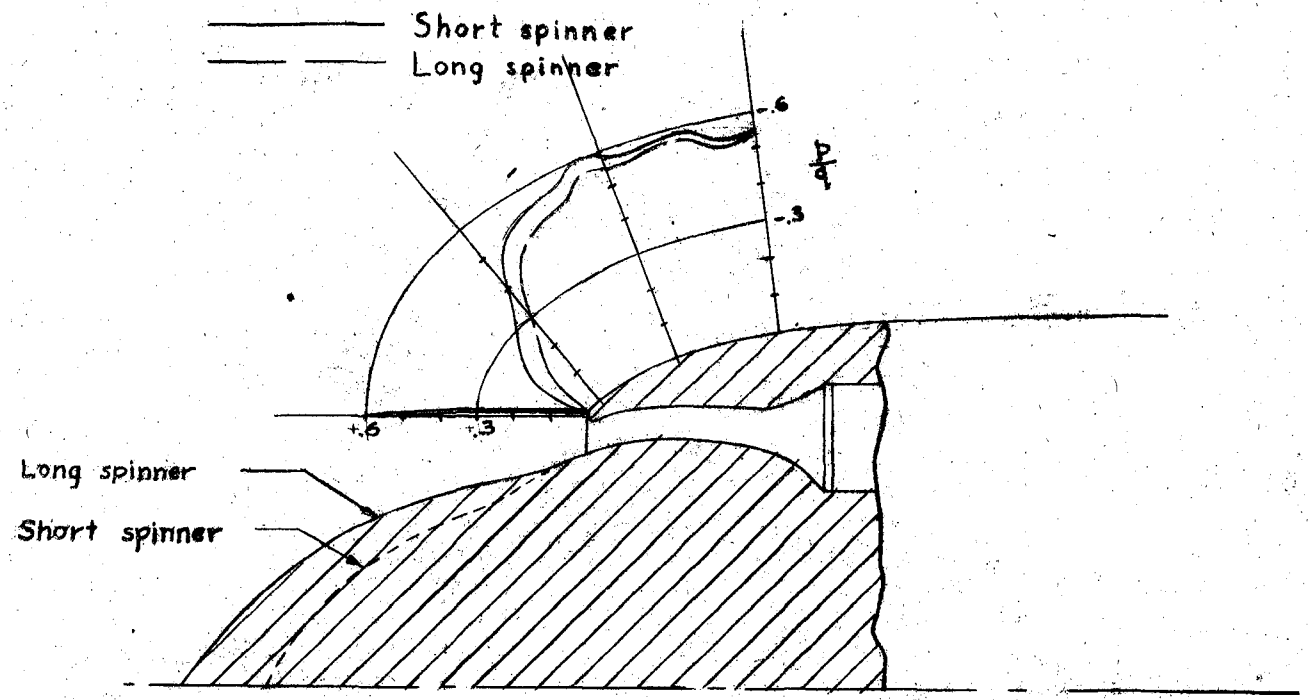

FIGURE 14.—Effect of spinner shape on pressure distribution on side of cowling. Angle of attack, 0°; V_i/V, 0.51.

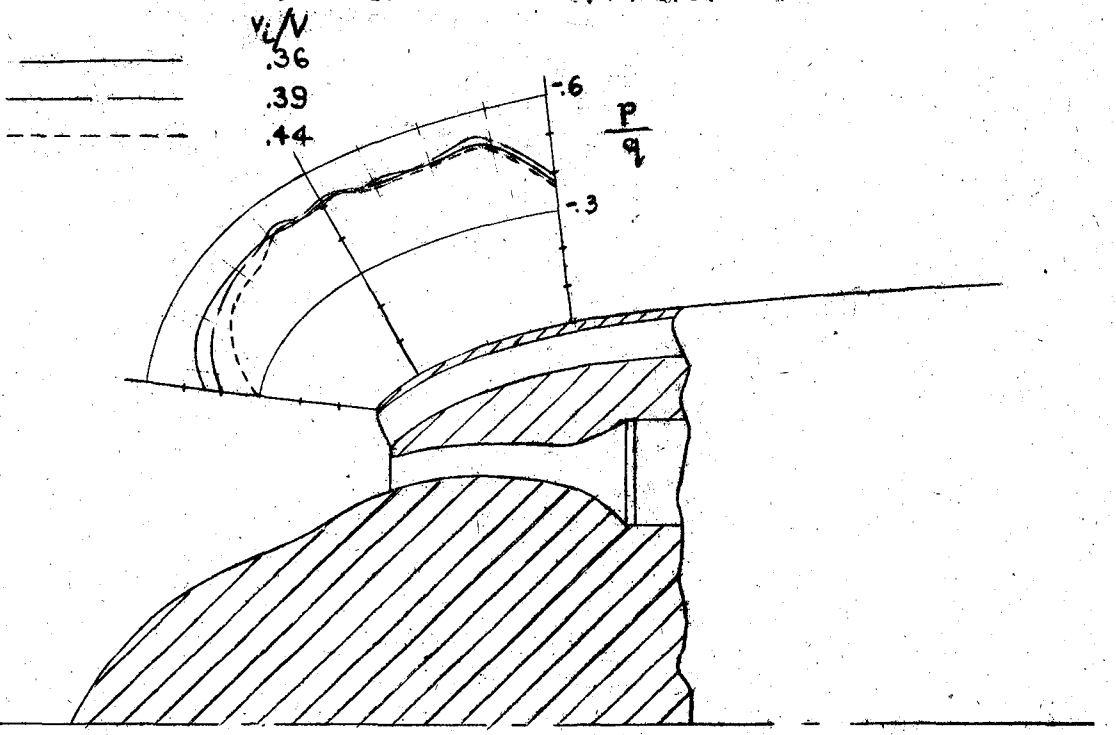

FIGURE 15.—Pressure distribution over top of carburetor air duct with short spinner. Angle of attack, 0°.

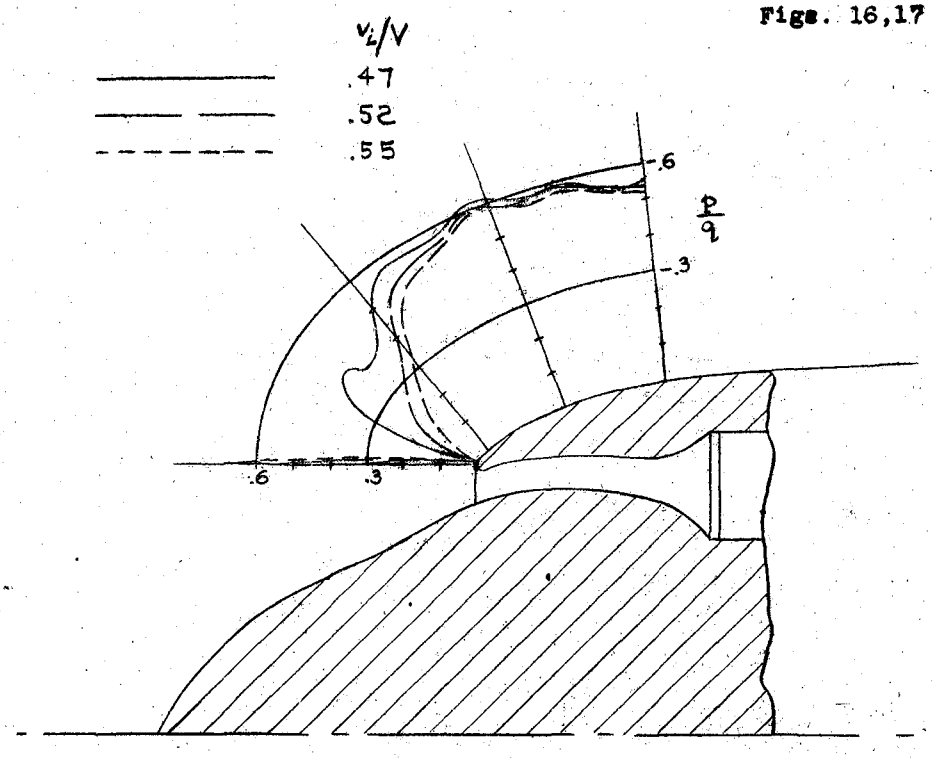

FIGURE 16.- Pressure distribution on side of cowling with short spinner. Angle of attack, 0°.

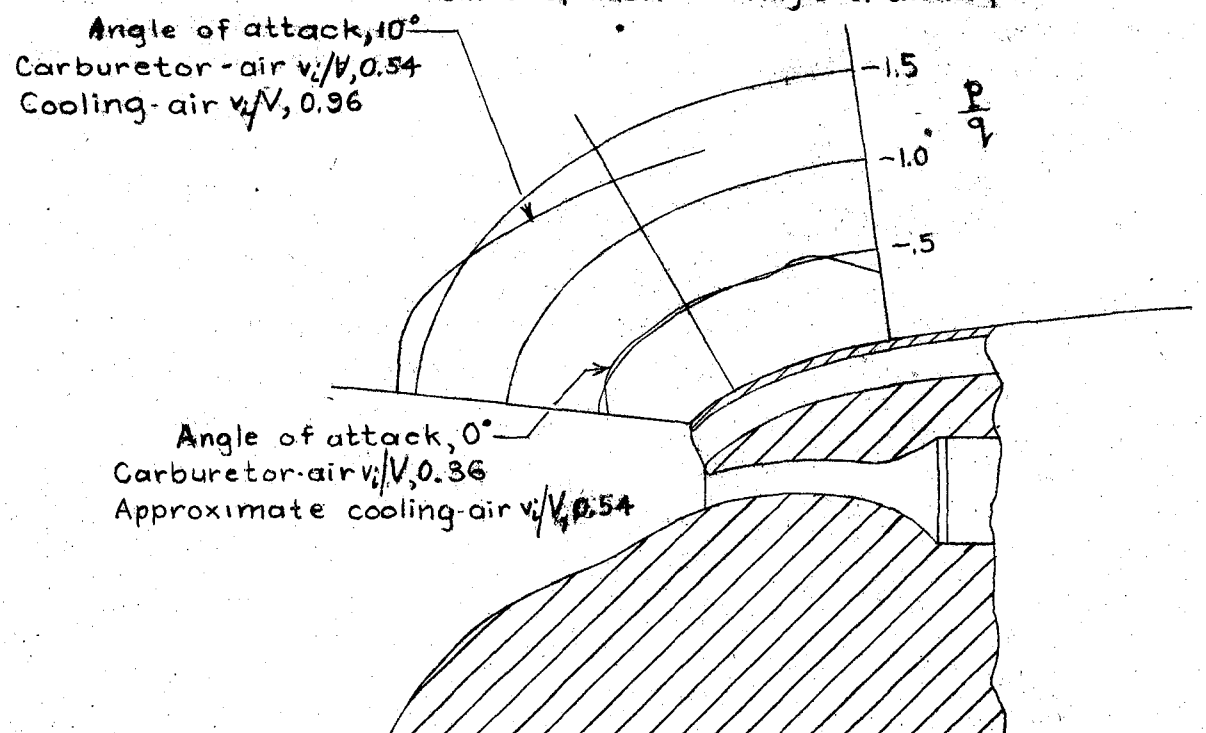

FIGURE 17.- Effect of angle of attack on pressure distribution over carburetor-air-duct outer surface with short spinner

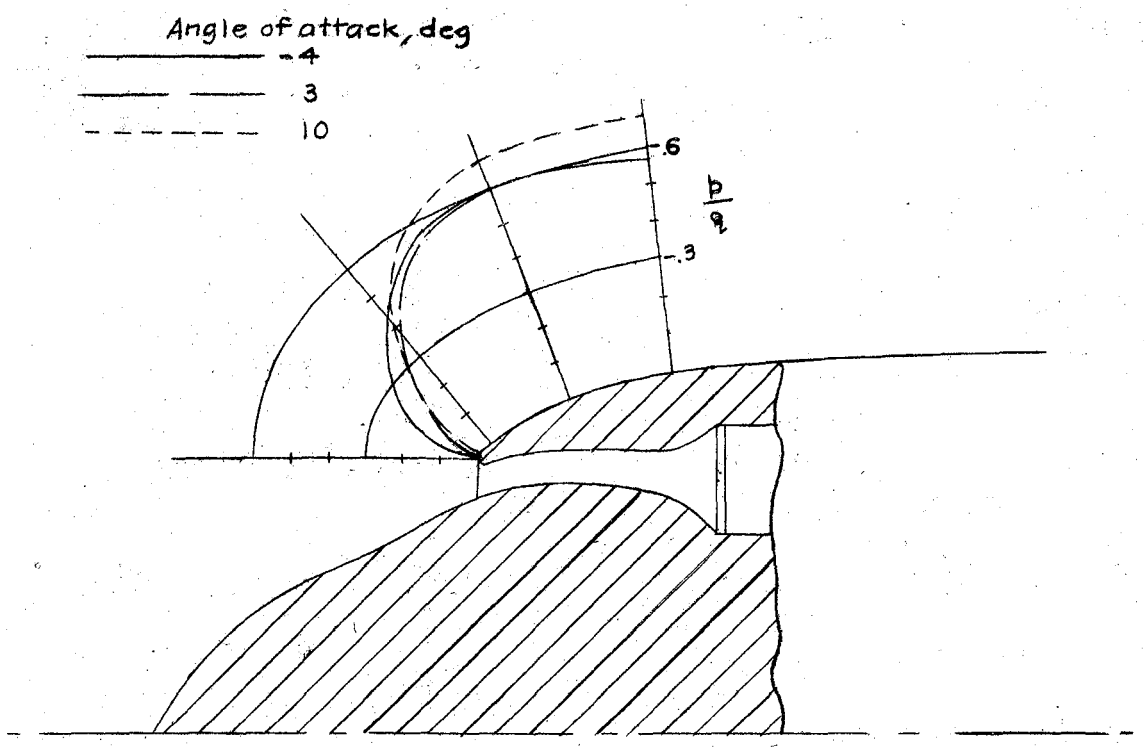

FIGURE 18.— Effect of angle of attack on pressure distribution over side of cowling with short spinner; A_e/F, 0.073.

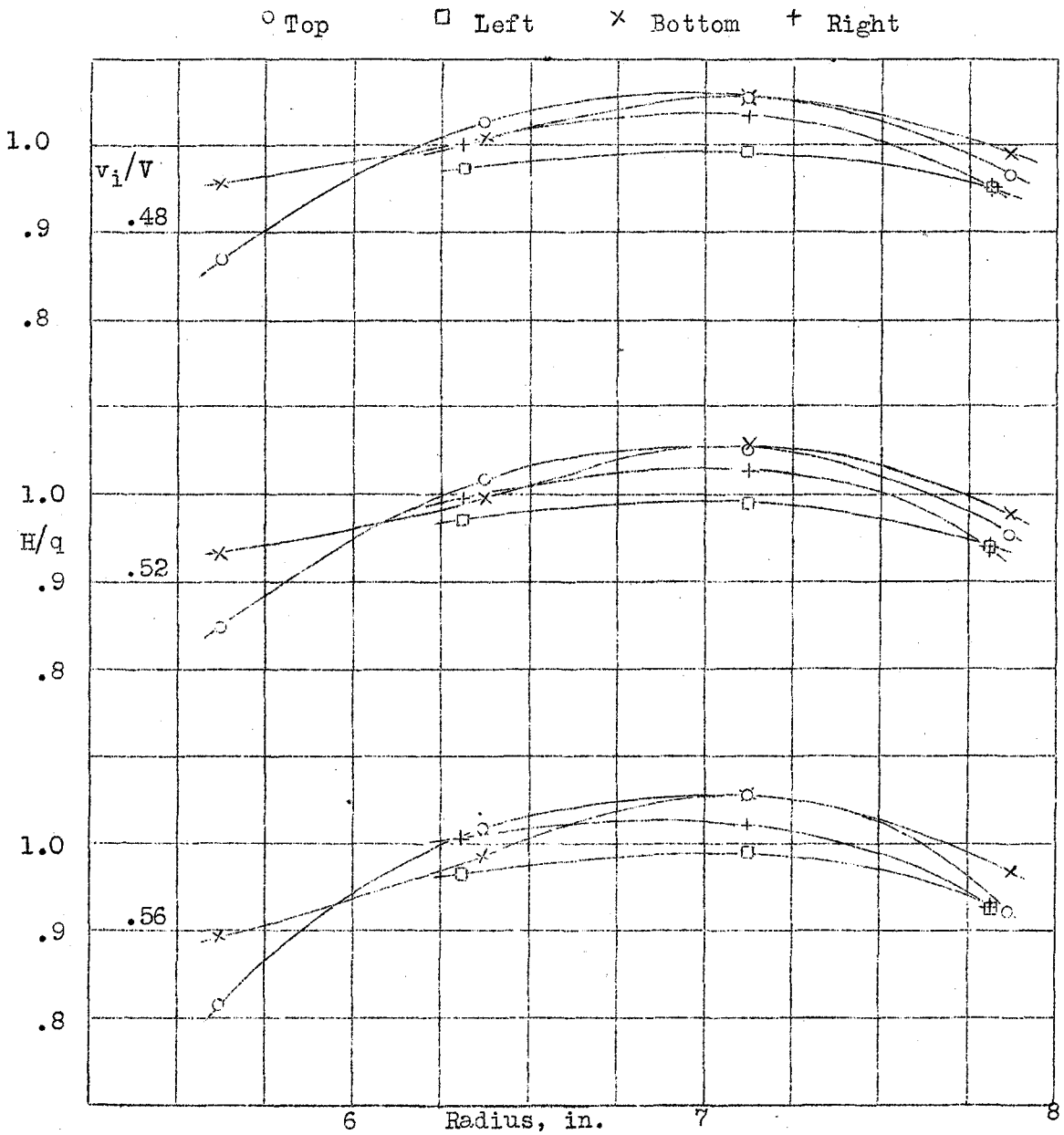

Figure 19.- Effect of inlet-velocity ratio on pressure distribution on orifice plate. Cowling D_s; propeller set 37.1°; angle of attack, 0°; V/nD, 1.7.

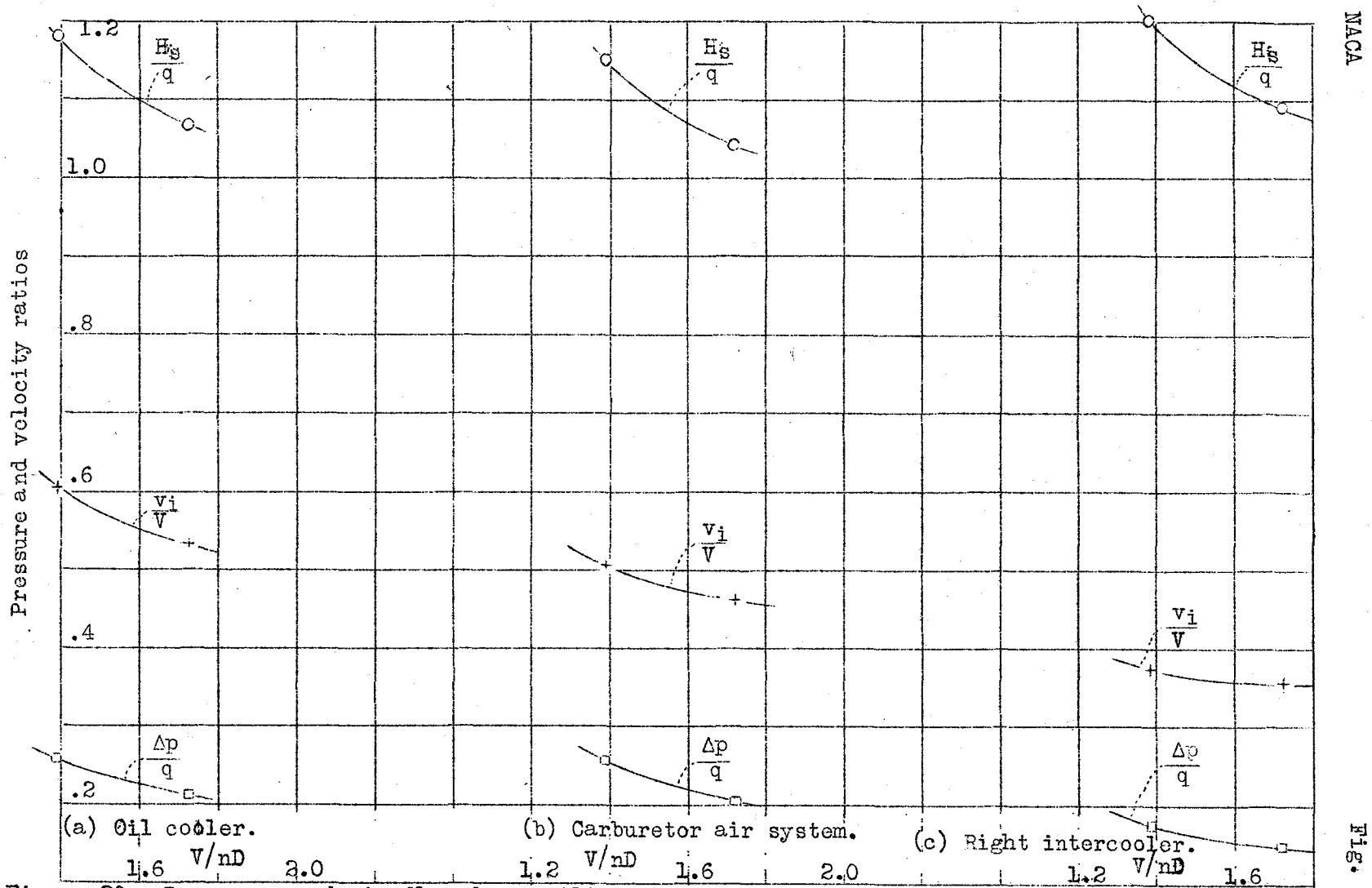

Figure 20.- Pressures and air flow for auxiliary internal-air systems. Cowling D_s; propeller set 37.1°; angle of attack, 0°; H_s, total pressure measured ahead of screen.

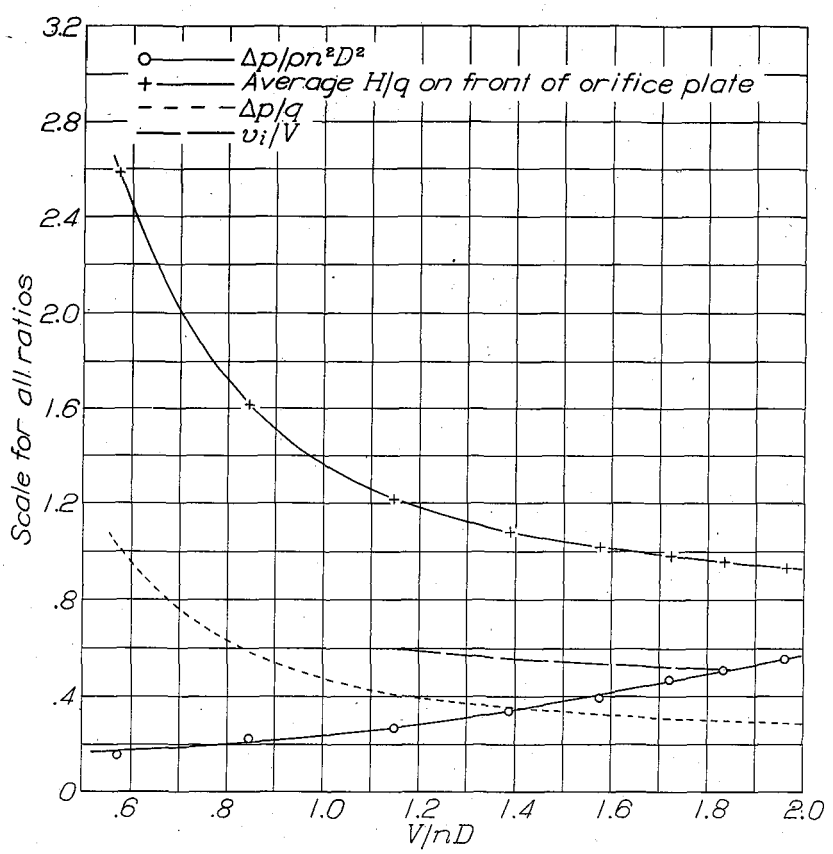

Figure 21.- Pressure coefficients for high-speed condition. Cowling D_s; propeller set 37.1°; angle of attack, 0°.

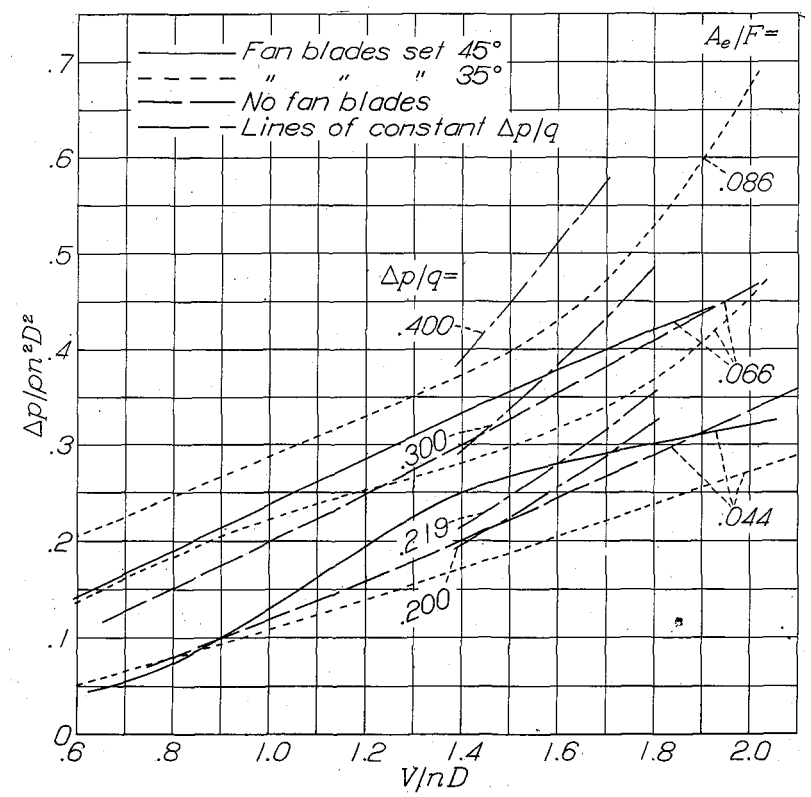

Figure 26.- Effect of fan blades on the internal pressure characteristics of cowling D_{sf}. Propeller set 37.1° with cuffs; angle of attack, 0°.

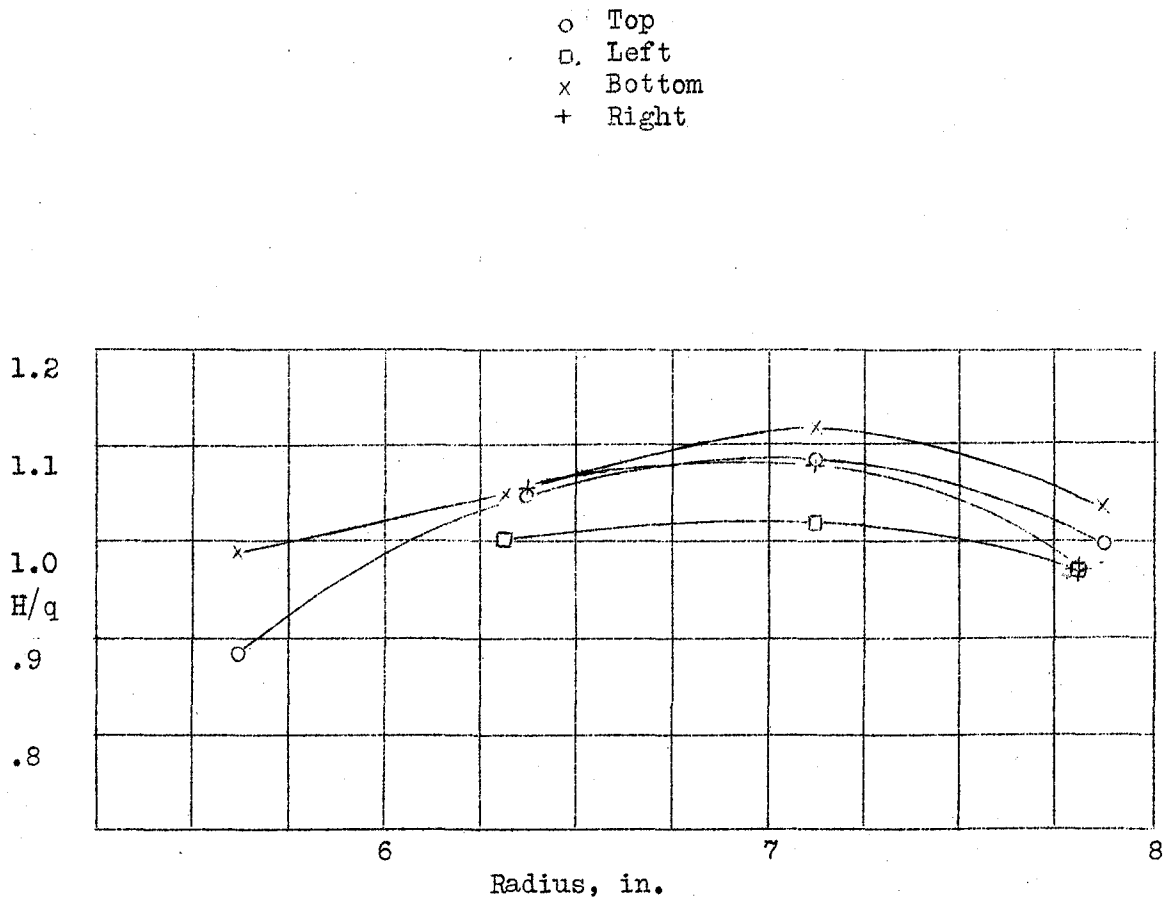

Figure 22.- Pressure distribution on orifice plate for high-speed condition. Cowling D_s; propeller set 37.1°; angle of attack, 0°; V/nD, 1.5; v_i/V, 0.54; $\Delta p/\rho n^2 D^2$, 0.380.

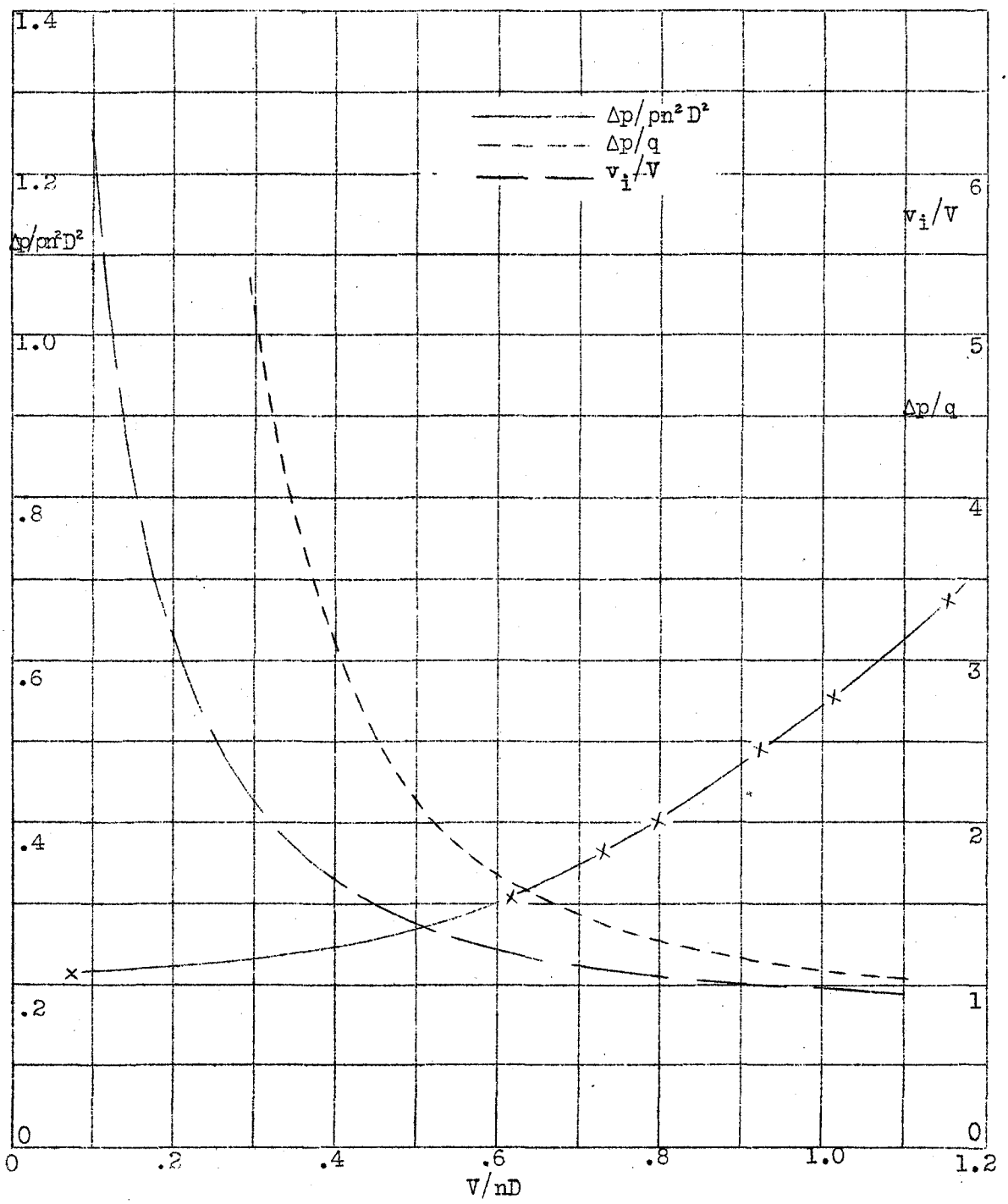

Figure 23.- Pressure-drop coefficient for take-off condition. Cowling D_s; propeller set 20°; angle of attack, 10°.

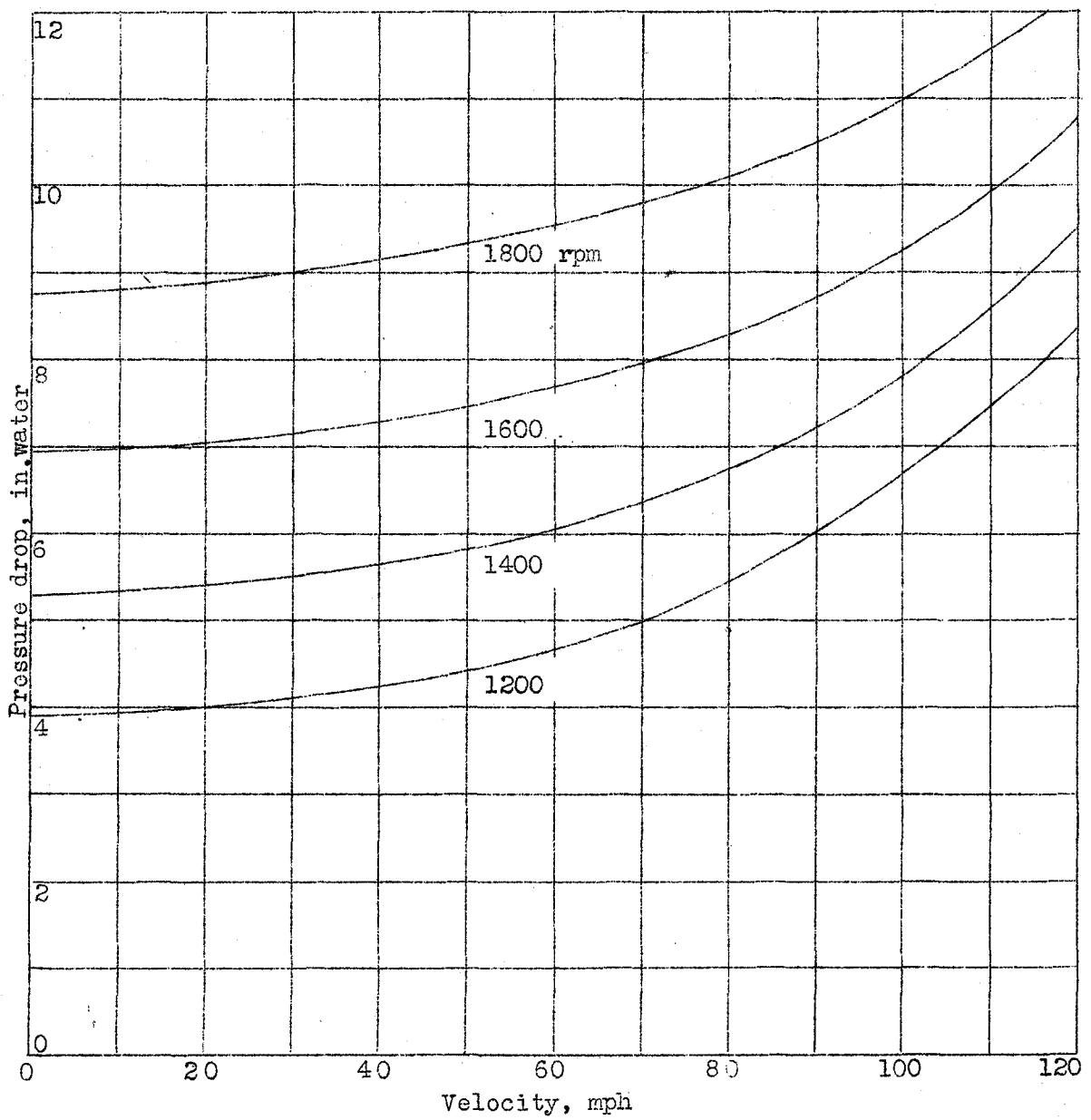

Figure 24.- Pressure drop with cowling D_s for full-scale airplane with 10-foot propeller set 20° with cuffs. $\rho = 0.002378$. Computed from pressure-drop coefficients obtained from Fig. 23.

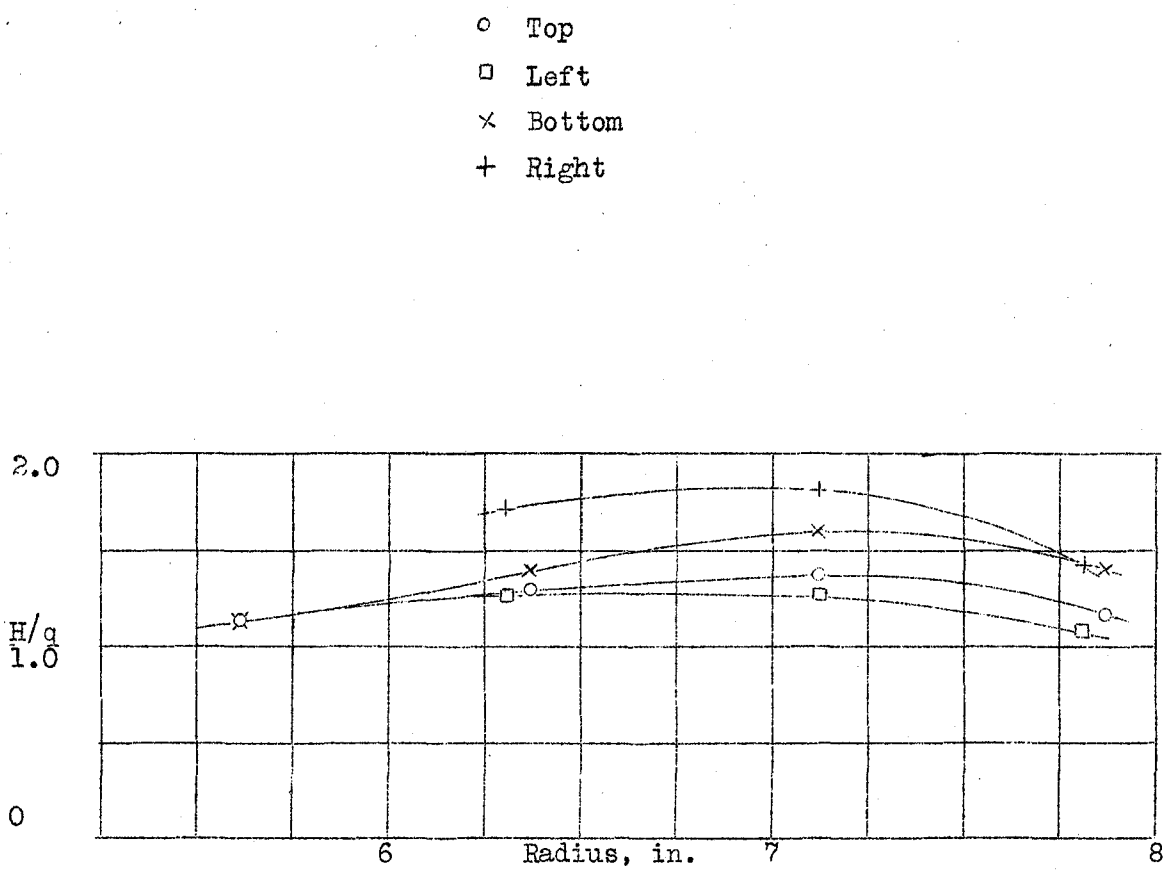

Figure 25.- Pressure distribution on orifice plate for take-off condition. Cowling D_s; propeller set 20°; angle of attack, 10°; V/nD, 0.65; v_i/V, 1.16.

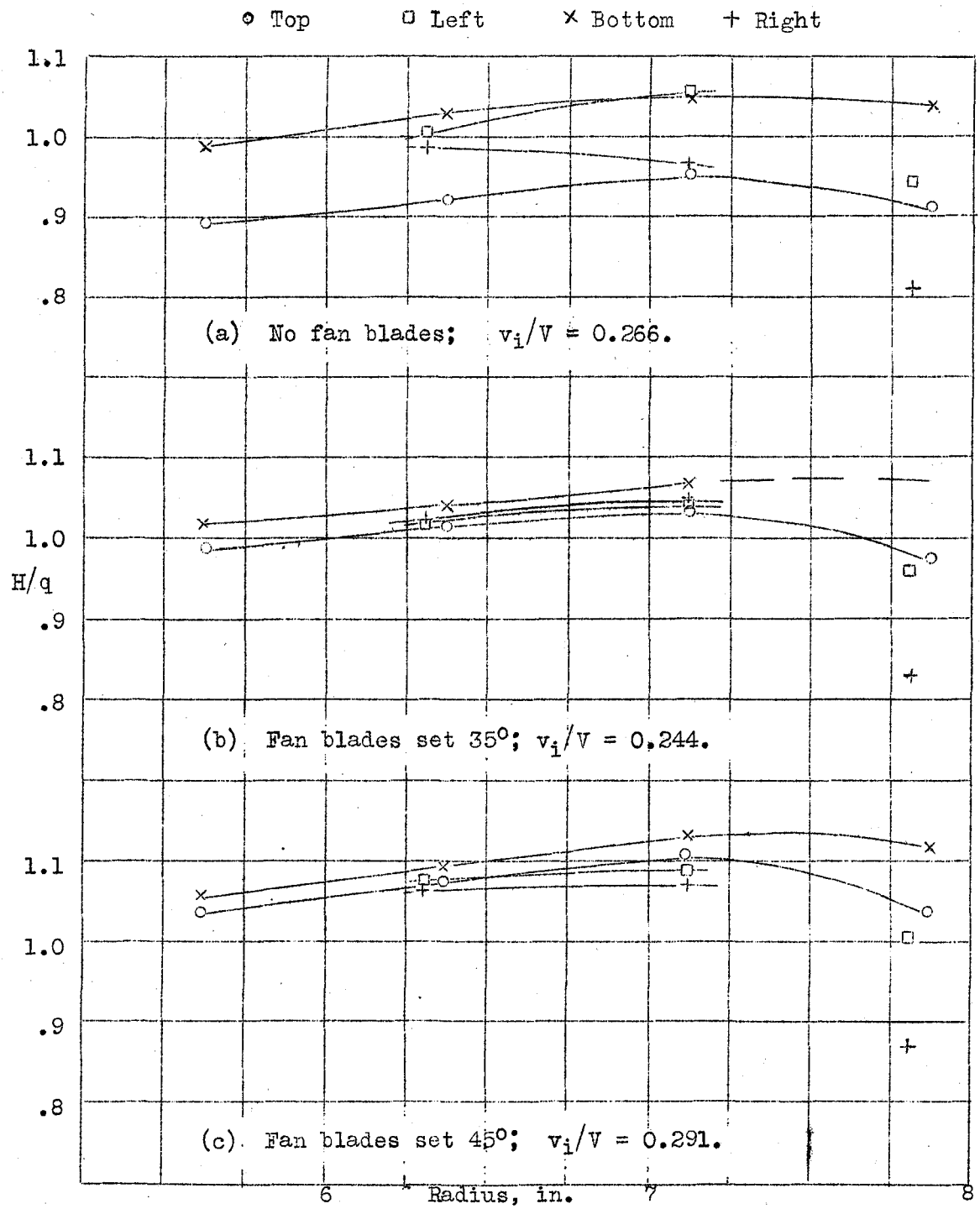

Figure 27.- Effect of fan blades on orifice-plate pressure distribution for cowling D_{sf}. Propeller set 37.1°; angle of attack, 0°; V/nD, 1.5; A_e/F, 0.044.

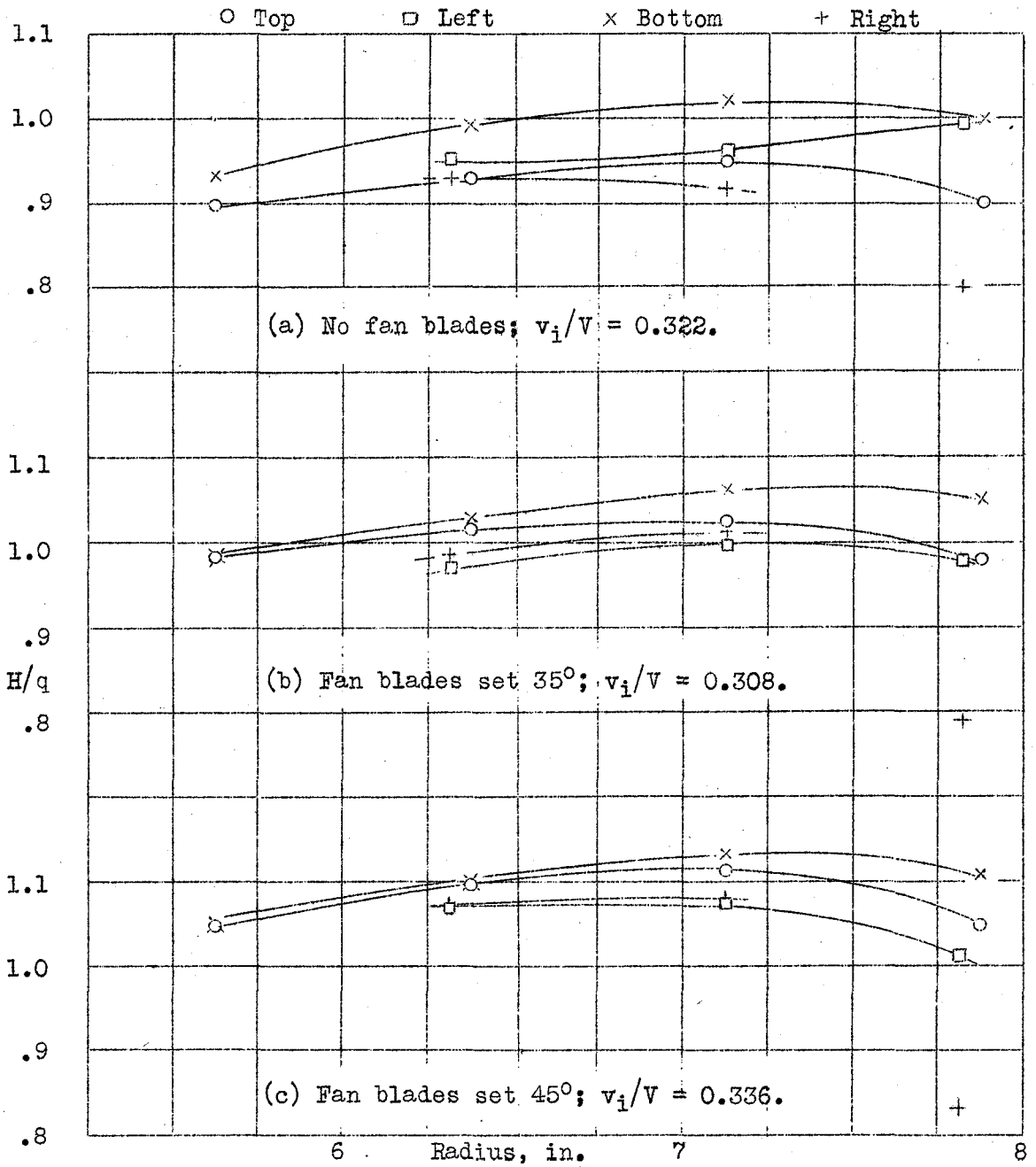

Figure 28.- Effect of fan blades on orifice-plate pressure distribution for cowling D_{sf}. Propeller set 37.1°; angle of attack, 0°; V/nD, 1.5; A_e/F, 0.066.

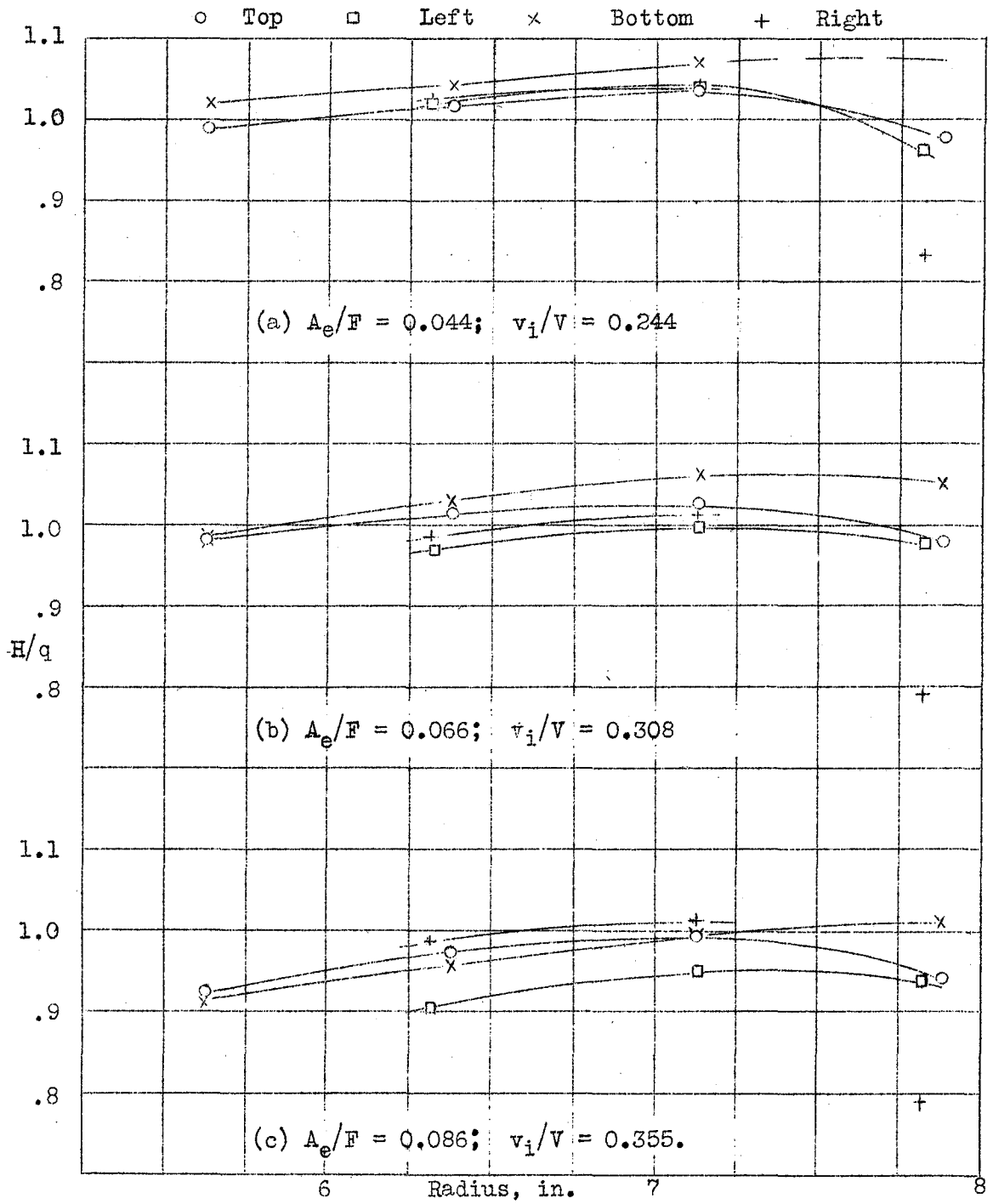

Figure 29.- Effect of fan blades on orifice-plate pressure distribution for cowling D_{sf}. Propeller set 37.1°; angle of attack, 0°; fan blades set 35°; V/nD, 1.5.

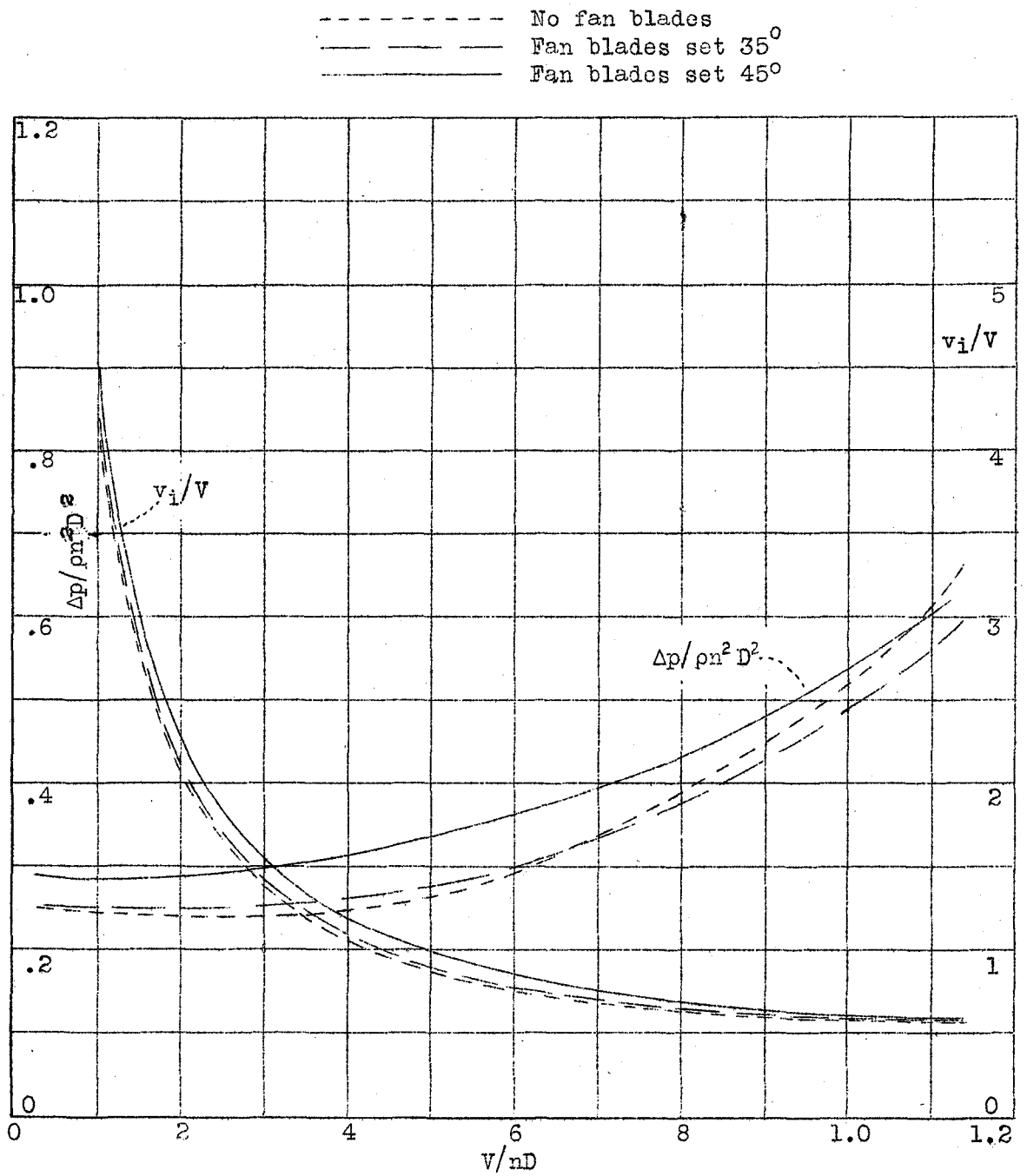

Figure 31.- Effect of fan blades on pressure drop for cowling D_{sf} in take-off condition. Propeller set 20° with cuffs; angle of attack, 10°; A_e/F, 0.220.

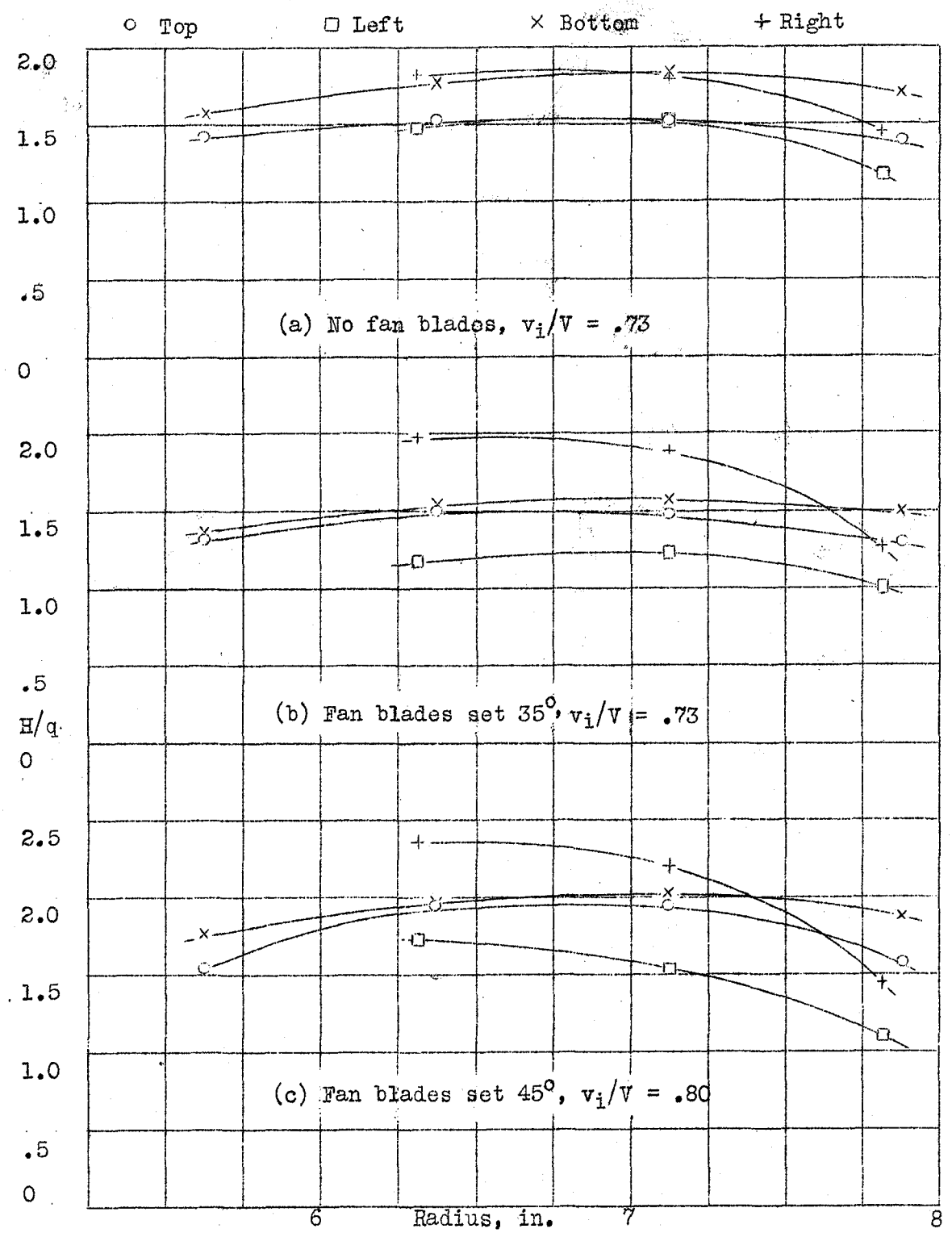

Figure 32.- Pressure distribution on orifice plate for take-off condition with cowling D_{sf}. Propeller set 20°; angle of attack, 10°; A_e/F, 0.220; V/nD, 0.65.

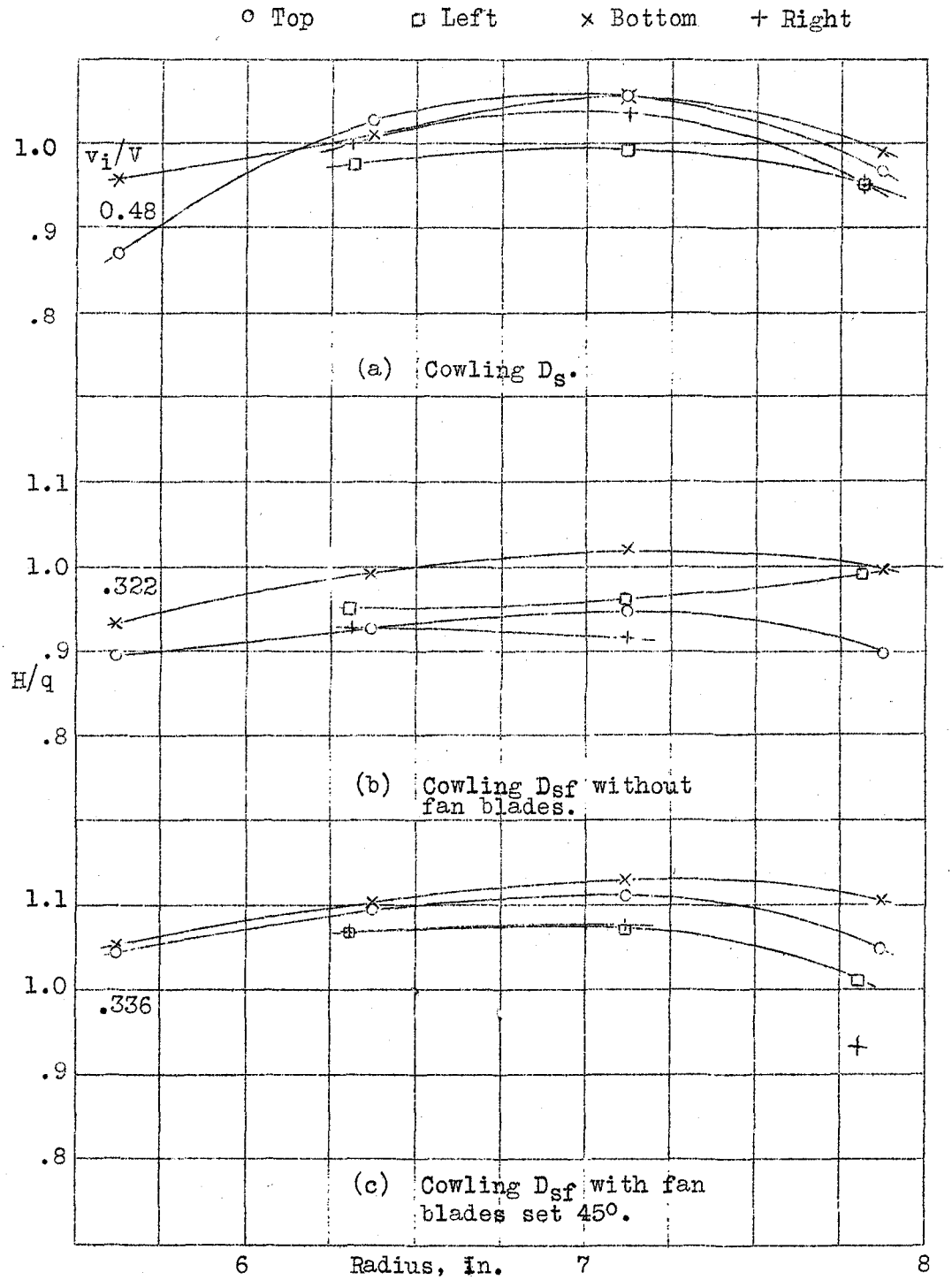

Figure 33.- Comparison of cowlings D_s and D_{sf} for the high-speed condition. Propeller set 37.1°; angle of attack, 0°; V/nD, 1.7.

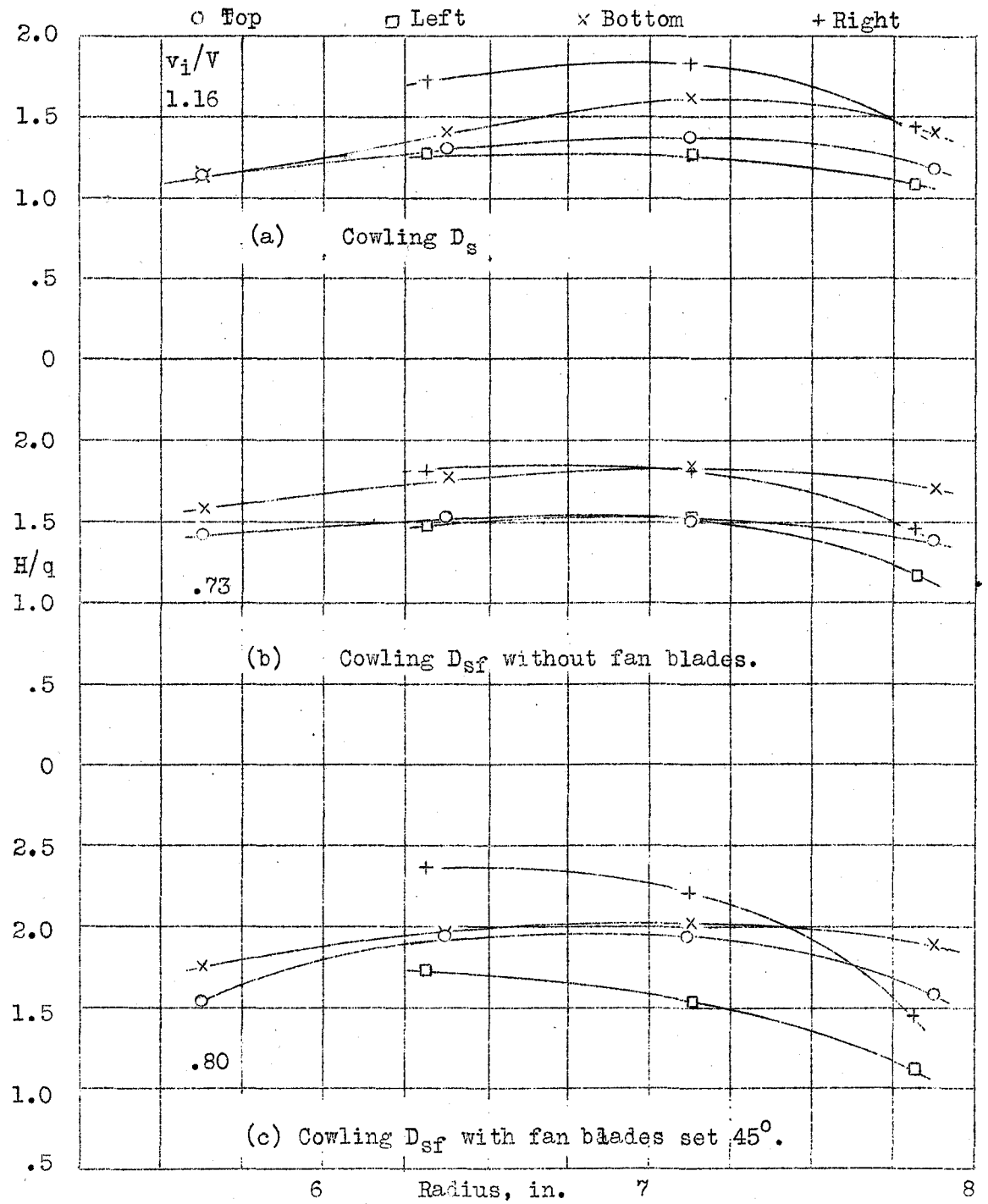

Figure 34.- Comparison of cowlings D_s and D_{sf} for the climb condition. Propeller set 20°; angle of attack, 10°; A_e/F, 0.220; V/nD, 0.65.